Hybrid Nonlinear Passivity-based Control Approach to Magnetic-Impulsive Spacecraft Attitude Regulation

Journal:	*Journal of Guidance, Control, and Dynamics*
Manuscript ID	2021-01-G005915.R2
Manuscript Type:	Full Paper
Date Submitted by the Author:	09-Feb-2024
Complete List of Authors:	Sharifi, Esmaeil; University of Toronto, Institute for Aerospace Studies Damaren, Christopher; University of Toronto, Institute for Aerospace Studies
Subject Index Category:	33300 Spacecraft Guidance and Control < 30000 GUIDANCE, CONTROL, AND DYNAMICS TECHNOLOGY

Hybrid Nonlinear Passivity-based Control Approach to Magnetic-Impulsive Spacecraft Attitude Regulation

Esmaeil Sharifi* and Christopher J. Damaren†
University of Toronto, Toronto, Ontario M3H 5T6, Canada

This paper proposes two novel passivity-based control design frameworks for hybrid nonlinear time-varying dynamical systems involving an interacting amalgam of continuous-time and discrete-time dynamics whose dynamical properties evolve periodically over time. In this regard, the hybrid Kalman-Yakubovich-Popov (KYP) conditions are employed in tandem with the passivity theorem to construct a three-step control design algorithm to render closed-loop dynamics stable. The proposed control architectures are subsequently exploited to regulate the attitude motion of spacecraft with magnetic and impulsive modes of operation. Practical considerations involved in implementing the proposed hybrid algorithms are then discussed in detail. Simulation results show significant improvement in the performance of the attitude control system in terms of system response, robustness, and the required magnetic and impulsive control usage as compared to a hybrid linear approach.

Nomenclature

$\mathcal{C}$	=	nonlinear passivity-based gain vector	$\boldsymbol{\varepsilon}$	=	vector part of quaternions
$\boldsymbol{P}$	=	linear passivity-based gain matrix	η	=	scalar part of quaternions
$\mathcal{P}$	=	linear strict passivity-based gain matrix	$\boldsymbol{\Phi}$	=	basis functions
$\boldsymbol{\Gamma}$	=	Riccati gain matrix	$\boldsymbol{\omega}$	=	angular velocity vector, rad/s

I. Introduction

HYBRID dynamical systems, as an emerging discipline within dynamical systems theory and control, comprise an interacting collection of dynamical systems involving a mixture of continuous-time and discrete-time dynamics. Possessing heterogeneous dynamics, the evolutions of which occur both continuously (flow) and discontinuously

* Ph.D. Candidate, Spacecraft Dynamics and Control Lab, Institute for Aerospace Studies. Student Member AIAA.
† Professor and Director, Institute for Aerospace Studies. Associate Fellow AIAA.

(jump) on appropriate manifolds over time, hybrid dynamical systems consist of three main elements: a continuous-time set of differential equations, which characterizes the motion of the dynamical system between impulsive events; a set of difference equations, which governs instantaneous changes in the states of the system when an impulse occurs; and a criterion to determine when impulses are to be applied (i.e. when the states of the system are to be reset) [1].

Motivated by applications of systems whose dynamical properties evolve over time, while simultaneously interacting with their surrounding environments, this paper proposes novel passivity-based control design architectures for hybrid nonlinear time-varying dynamical systems. The proposed hybrid control schemes are subsequently utilized to regulate the attitude motion of spacecraft under a hybrid source of actuation. The notion of passivity provides a fundamental framework for the analysis and control design of dynamical systems via exerting a constraint on the amount of energy they exchange through their input-output ports. The origin of this concept can be traced back to development in the linear passive network theory in the 1950s [2] and, specifically, the stability analysis of feedback systems through positive real matrices in the 1960s [3-5]. Nevertheless, the first general input-output energy-based system description was proposed by J. Willems in 1972 via introducing the dissipativity theory for linear dynamical systems [6, 7]. This pioneering work was then followed by characterizing dissipativeness in an input-output sense for a large class of nonlinear systems [8-10]. Providing a generalized interpretation of energy balance in terms of the stored energy and the dissipated energy over heterogeneous dynamics, the dissipativity theory was then generalized to hybrid nonlinear time-invariant dynamical systems with an interacting mixture of continuous-time and discrete-time dynamics in Ref. [11].

Although the control theory for hybrid nonlinear dissipative dynamical systems is well-developed (See Ref. [1] and references therein), there have been no applications due primary to a lack of efficient numerical schemes for dealing effectively with such systems. This paper aims to bridge the gap between theory and practice by developing two novel passivity-based control design frameworks for hybrid nonlinear time-varying dynamical systems involving an interacting amalgam of continuous-time and discrete-time dynamics whose dynamical properties evolve periodically over time. In this regard, the Kalman-Yakubovich-Popov (KYP) conditions characterizing dissipativity properties for hybrid nonlinear time-varying dynamical systems and the passivity theorem (Refer to Ref. [2] for the original form and to Ref. [12] for the extended hybrid version) are collaboratively utilized to develop a three-step control design algorithm. To accord with the passivity theorem, which necessitates interconnecting a passive plant with an input strictly passive controller through negative feedback to yield a stable closed-loop system,

the hybrid output of the plant is first determined judiciously to satisfy the passivity specifications via the corresponding KYP conditions. A hybrid nonlinear controller, which separately adopts compensators of static and dynamic structures, is then designed to meet the strict passivity requirements. The stability of the closed-loop system is consequently established by a negative feedback interconnection of the (passive) plant and the (input strictly passive) controller. The proposed hybrid control algorithms are ultimately exploited to regulate the attitude motion of spacecraft, the rotational kinematics and dynamics of which form a dynamical system of a highly nonlinear nature, with two modes of operation, namely magnetic actuation and impulsive thrusts.

Magnetic actuation originating from the interaction between the onboard electromagnetic dipole moments and the Earth's magnetic field is essentially based upon simple principles of physics: a planar loop of area $\mathcal{A}$ with $\mathcal{N}$ turns of wire carrying a current of $\mathcal{I}$ produces a magnetic dipole moment of magnitude $\mathcal{NIA}$ in the direction normal to the plane of the loop satisfying a right-hand rule; when the magnetic dipole moment generated onboard via current-carrying coils of wire is immersed in the geomagnetic field, a magnetic torque is consequently produced in the direction (plane) orthogonal to the Earth's magnetic field [13-15]. The resultant magnetic torque can therefore be used as an actuation mechanism for detumbling of spacecraft [16] and momentum dumping of reaction wheels [17]. A survey of control design techniques developed for magnetic spacecraft attitude control can be found in Ref. [18].

Magnetic attitude control systems benefit from several advantages for near-Earth missions; including an essentially unlimited mission life due to use of a renewable source of actuation, the absence of catastrophic failure modes, the smoothness of application, and significant savings in the overall weight and complexity of the system owing to the absence of moving parts [14-16]. On the other hand, magnetically actuated control systems suffer inherently from instantaneous underactuation stemming from orthogonality of the magnetic control torque to the instantaneous direction of the Earth's magnetic field (due to the cross product between the magnetic dipole moment vector and the magnetic field vector from which magnetic actuation originates). Controllability in such systems, therefore, depends on orbit characteristics and the location of spacecraft in the orbit [14, 15]. Furthermore, the time-varying nature of the magnetic actuation mechanism, which arises from the variations of the Earth's magnetic field along the spacecraft orbit, effectively gives rise to time-varying control gains. Stability considerations impose limitations on the size of these gains which ultimately limits the performance of the closed-loop system [19]. As another disadvantage, magnetic actuators only offer slow attitude maneuvers and stabilization which, in turn, restricts their range of application [14].

To resolve these drawbacks, which pertain inherently to magnetic actuation, magnetic attitude controllers have been employed in conjunction with additional attitude stabilization mechanisms, from passive to active. Spin stabilization [20], dual-spin stabilization [21], and gravity-gradient stabilization [22] describe techniques of a passive nature used collaboratively to support magnetic actuation; whereas reaction wheels [23, 24] and thrusters [12, 25, 26] present common mechanisms to actively complement magnetic control. Collaborative application of magnetic and mechanical actuation has also been used in practice to rescue spacecraft in orbit after hardware failures in their attitude control systems. For instance, after an unforeseen occurrence of uncontrollability in the pitch axis of RADARSAT-1 due to failure in its primary and secondary pitch axis wheels, three-axis control was restored through utilizing magnetic actuation in tandem with reaction wheels [27].

In this paper, impulsive thrusting is employed as an auxiliary actuation mechanism to collaboratively augment magnetic actuation in order to, amongst other objectives, improve the performance of the attitude control system. Aiming to design an attitude controller with enhanced capabilities in terms of operating range, gain margin, and robustness for the resultant hybrid time-varying dynamical system, a nonlinear passivity-based control approach is then adopted to attain the main objective, that is, to regulate the attitude motion of spacecraft subject to gravity-gradient disturbances and residual magnetic dipole moments resulting from onboard electronics. By making use of the control scheme proposed in this research work, not only are the aforementioned inherent drawbacks involved in magnetically actuated dynamical systems effectively resolved, but the feedback attitude controller required to stabilize the spacecraft attitude control system is also synthesized by considering the full nonlinear kinematics and dynamics of the system. No linearization is involved, neither dynamic feedback linearization nor a priori linearization of the rotational equations of motion. Therefore, the attitude control system equipped with a nonlinear controller is no longer restricted to operate in the vicinity of the equilibrium and can be exploited over the entire operating range of the system. This, in consequence, reduces the complexity and cost of the system, while simultaneously increasing the functional performance. Moreover, due to utilizing a passivity-based control approach, the resultant attitude control system is expected to exhibit enhanced robustness properties.

This paper is organized as follows. The preliminary definitions and main theorems associated with hybrid nonlinear dissipative dynamical systems are presented in Sec. II. Two novel passivity-based control design frameworks are then developed for hybrid nonlinear time-varying dynamical systems in Sec. III. The kinematic and dynamic equations of motion characterizing the cascade nature of the spacecraft attitude motion are then reviewed in Sec. IV. Section V describes practical considerations involved in implementing the proposed hybrid control

algorithms. The control algorithms developed in Sec. III are ultimately utilized to regulate the attitude motion of spacecraft with magnetic and impulsive modes of operations in Sec. VI.

II. Hybrid Nonlinear Dissipative Dynamical Systems

This section aims to provide a sound base from which the desired passivity-based control design frameworks are developed for hybrid nonlinear dynamical systems whose dynamical properties evolve over time. Consider a hybrid dynamical system $\mathcal{G}$ modeled by nonlinear equations of the form:

$$\dot{\boldsymbol{x}}(t) = \boldsymbol{f}_{ct}(\boldsymbol{x},t) + \boldsymbol{g}_{ct}(\boldsymbol{x},t)\boldsymbol{u}_{ct}(t) \;,\; \boldsymbol{x}(\boldsymbol{0}) = \boldsymbol{x}_0 \qquad t \neq t_k \tag{1}$$

$$\boldsymbol{y}_{ct}(t) = \boldsymbol{h}_{ct}(\boldsymbol{x},t) + \boldsymbol{j}_{ct}(\boldsymbol{x},t)\boldsymbol{u}_{ct}(t) \qquad t \neq t_k \tag{2}$$

$$\boldsymbol{x}_k^+ = \boldsymbol{f}_{ds}(\boldsymbol{x}_k^-,t) + \boldsymbol{g}_{ds}(\boldsymbol{x}_k^-,t)\boldsymbol{u}_{ds}(t) \qquad t = t_k \tag{3}$$

$$\boldsymbol{y}_{ds}(t) = \boldsymbol{h}_{ds}(\boldsymbol{x}_k^-,t) + \boldsymbol{j}_{ds}(\boldsymbol{x}_k^-,t)\boldsymbol{u}_{ds}(t) \qquad t = t_k \tag{4}$$

where $t \geq 0$, $\boldsymbol{x} \in \mathcal{D} \subseteq \mathbb{R}^n$ is the state vector, $\mathcal{D}$ specifies an open set with $\boldsymbol{0} \in \mathcal{D}$ defined as the state space of interest, $\boldsymbol{f}_{ct} : \mathcal{D} \times \mathbb{R} \to \mathbb{R}^n$ is Lipschitz continuous on $\mathcal{D}$, $\boldsymbol{g}_{ct} : \mathcal{D} \times \mathbb{R} \to \mathbb{R}^{n \times m_{ct}}$, $\boldsymbol{u}_{ct} \in \boldsymbol{U}_{ct} \subseteq \mathbb{R}^{m_{ct}}$ denotes the continuous-time control input, $\boldsymbol{y}_{ct} \in \boldsymbol{Y}_{ct} \subseteq \mathbb{R}^{q_{ct}}$ is the continuous-time output, $\boldsymbol{h}_{ct} : \mathcal{D} \times \mathbb{R} \to \mathbb{R}^{q_{ct}}$, $\boldsymbol{j}_{ct} : \mathcal{D} \times \mathbb{R} \to \mathbb{R}^{q_{ct} \times m_{ct}}$, t_k indicates the time instants at which impulses are applied with $k \in \mathbb{Z}_{(t_0,t_f)} \triangleq \{k : t_0 < t_k < t_f\}$, $\boldsymbol{x}_k^- \triangleq \boldsymbol{x}(t_k^-)$ and $\boldsymbol{x}_k^+ \triangleq \boldsymbol{x}(t_k^+)$ denote the state vector immediately before and after discrete-time dynamics are excited at $t = t_k$ respectively, $\boldsymbol{f}_{ds} : \mathcal{D} \times \mathbb{R} \to \mathbb{R}^n$ is continuous on $\mathcal{D}$, $\boldsymbol{g}_{ds} : \mathcal{D} \times \mathbb{R} \to \mathbb{R}^{n \times m_{ds}}$, $\boldsymbol{u}_{ds} \in \boldsymbol{U}_{ds} \subseteq \mathbb{R}^{m_{ds}}$ specifies the discrete-time control input, $\boldsymbol{y}_{ds} \in \boldsymbol{Y}_{ds} \subseteq \mathbb{R}^{q_{ds}}$ is the discrete-time output, $\boldsymbol{h}_{ds} : \mathcal{D} \times \mathbb{R} \to \mathbb{R}^{q_{ds}}$, and $\boldsymbol{j}_{ds} : \mathcal{D} \times \mathbb{R} \to \mathbb{R}^{q_{ds} \times m_{ds}}$. Note that the subscripts "*ct*" and "*ds*" refer to the quantities in the continuous-time and discrete-time subsystems, respectively.

A. Preliminary Definitions

Presenting the key definitions relevant to dissipativeness, this section paves the way for developing the KYP conditions in question for hybrid nonlinear time-varying dynamical systems as follows.

Definition 1: For the hybrid dynamical system $\mathcal{G}$ given by Eqs. (1)-(4), a function $\big(S_{ct}(\boldsymbol{u}_{ct},\boldsymbol{y}_{ct}), S_{ds}(\boldsymbol{u}_{ds},\boldsymbol{y}_{ds})\big)$, where $S_{ct} : \boldsymbol{U}_{ct} \times \boldsymbol{Y}_{ct} \to \mathbb{R}$ and $S_{ds} : \boldsymbol{U}_{ds} \times \boldsymbol{Y}_{ds} \to \mathbb{R}$ are such that $S_{ct}(\boldsymbol{0},\boldsymbol{0}) = 0$ and $S_{ds}(\boldsymbol{0},\boldsymbol{0}) = 0$, is called a *hybrid supply*

rate if, for all input-output pairs $(\boldsymbol{u}_{ct}, \boldsymbol{y}_{ct}) \in (\boldsymbol{U}_{ct}, \boldsymbol{Y}_{ct})$ and $(\boldsymbol{u}_{ds}, \boldsymbol{y}_{ds}) \in (\boldsymbol{U}_{ds}, \boldsymbol{Y}_{ds})$ satisfying Eqs. (1)-(4) and for $k \in \mathbb{Z}_{(\tau_1,\tau_2)} \triangleq \{k : \tau_1 < t_k < \tau_2\}$, $S_{ct}(\boldsymbol{u}_{ct}, \boldsymbol{y}_{ct})$ and $S_{ds}(\boldsymbol{u}_{ds}, \boldsymbol{y}_{ds})$ benefit from the following properties [1]:

$$\int_{\tau_1}^{\tau_2} \left| S_{ct}\left(\boldsymbol{u}_{ct}(t), \boldsymbol{y}_{ct}(t)\right) \right| dt < \infty \quad \forall \tau_1, \tau_2 \geq 0 \tag{5}$$

$$\sum\nolimits_{k \in \mathbb{Z}_{(\tau_1,\tau_2)}} \left| S_{ds}\left(\boldsymbol{u}_{ds}(t_k), \boldsymbol{y}_{ds}(t_k)\right) \right| < \infty \tag{6}$$

Definition 2: The hybrid dynamical system $\mathcal{G}$ with $m_{ct} = q_{ct}$, $m_{ds} = q_{ds}$, and $\boldsymbol{x}(t_0) = \boldsymbol{0}$ is *passive* if for all $\tau \geq t_0$

$$\int_{t_0}^{\tau} \boldsymbol{y}_{ct}^{\mathrm{T}}(t)\boldsymbol{u}_{ct}(t)dt + \sum\nolimits_{k \in \mathbb{Z}_{(t_0,\tau)}} \boldsymbol{y}_{ds}^{\mathrm{T}}(t_k)\boldsymbol{u}_{ds}(t_k) \geq 0 \tag{7}$$

Definition 3: The hybrid dynamical system $\mathcal{G}$ with $m_{ct} = q_{ct}$, $m_{ds} = q_{ds}$, and $\boldsymbol{x}(t_0) = \boldsymbol{0}$ is *input strictly passive* if there exist $\gamma_{ct} > 0$ and $\gamma_{ds} > 0$ such that for all $\tau \geq t_0$

$$\int_{t_0}^{\tau} \boldsymbol{y}_{ct}^{\mathrm{T}}(t)\boldsymbol{u}_{ct}(t)dt + \sum\nolimits_{k \in \mathbb{Z}_{(t_0,\tau)}} \boldsymbol{y}_{ds}^{\mathrm{T}}(t_k)\boldsymbol{u}_{ds}(t_k) \geq \gamma_{ct} \int_{t_0}^{\tau} \boldsymbol{u}_{ct}^{\mathrm{T}}(t)\boldsymbol{u}_{ct}(t)dt + \gamma_{ds} \sum\nolimits_{k \in \mathbb{Z}_{(t_0,\tau)}} \boldsymbol{u}_{ds}^{\mathrm{T}}(t_k)\boldsymbol{u}_{ds}(t_k) \tag{8}$$

Definition 4: Consider the hybrid dynamical system $\mathcal{G}$ with the hybrid supply rate $\left(S_{ct}(\boldsymbol{u}_{ct}, \boldsymbol{y}_{ct}), S_{ds}(\boldsymbol{u}_{ds}, \boldsymbol{y}_{ds})\right)$. A continuous positive semi-definite function $V : \mathcal{D} \times \mathbb{R} \to \mathbb{R}$ satisfying $V(\boldsymbol{0}, t) = 0$ for all $t \in \mathbb{R}$ and

$$\int_{t_0}^{\tau} S_{ct}\left(\boldsymbol{u}_{ct}(t), \boldsymbol{y}_{ct}(t)\right) dt + \sum\nolimits_{k \in \mathbb{Z}_{(t_0,\tau)}} S_{ds}\left(\boldsymbol{u}_{ds}(t_k), \boldsymbol{y}_{ds}(t_k)\right) \geq V\left(\boldsymbol{x}(\tau), \tau\right) - V\left(\boldsymbol{x}(t_0), t_0\right) \tag{9}$$

is called a *storage function* for $\mathcal{G}$, wherein $\boldsymbol{x}(t)$ for $\tau \geq t_0$ is a solution to Eqs. (1)-(4) with $(\boldsymbol{u}_{ct}, \boldsymbol{u}_{ds}) \in \boldsymbol{U}_{ct} \times \boldsymbol{U}_{ds}$ [1].

Definition 5: The $\mathcal{L}_2$ and ℓ_2 spaces are, respectively, defined as the space of all square-integrable continuous-time and square-summable discrete-time vector functions as $\mathcal{L}_2 \triangleq \left\{ \boldsymbol{u}_{ct}(t) \in \boldsymbol{U}_{ct} \middle| \int_0^{\infty} \boldsymbol{u}_{ct}^{\mathrm{T}}(t)\boldsymbol{u}_{ct}(t)\mathrm{d}t < \infty \right\}$ and $\ell_2 \triangleq \left\{ \boldsymbol{u}_{ds}(t_k) \in \boldsymbol{U}_{ds} \middle| \sum_{k=1}^{\infty} \boldsymbol{u}_{ds}^{\mathrm{T}}(t_k)\boldsymbol{u}_{ds}(t_k) < \infty \right\}$, where $k \in \mathbb{Z}^+$ [1].

Definition 6: The continuous-time system $\boldsymbol{y}_{ct} = \mathcal{G}_{ct}\boldsymbol{u}_{ct}$, with $\boldsymbol{u}_{ct} \in \boldsymbol{U}_{ct} \subseteq \mathbb{R}^{m_{ct}}$ as the control input and $\boldsymbol{y}_{ct} \in \boldsymbol{Y}_{ct} \subseteq \mathbb{R}^{q_{ct}}$ as the output, is *Input-Output* $\mathcal{L}_2$ *stable* if having $\|\boldsymbol{u}_{ct}\| \in \mathcal{L}_2$ implies $\|\boldsymbol{y}_{ct}\| \in \mathcal{L}_2$ as well. Similarly, the discrete-time system $\boldsymbol{y}_{ds} = \mathcal{G}_{ds}\boldsymbol{u}_{ds}$ with $\boldsymbol{u}_{ds} \in \boldsymbol{U}_{ds} \subseteq \mathbb{R}^{m_{ds}}$ as the control input and $\boldsymbol{y}_{ds} \in \boldsymbol{Y}_{ds} \subseteq \mathbb{R}^{q_{ds}}$ as the output is *Input-Output* ℓ_2 *stable* if having $\|\boldsymbol{u}_{ds}\| \in \ell_2$ implies $\|\boldsymbol{y}_{ds}\| \in \ell_2$ as well [1].

The required tools are now in place to derive the KYP conditions for hybrid nonlinear time-varying dynamical systems. This objective is attained in the next section.

B. Hybrid Nonlinear Time-varying KYP Conditions

This section serves to characterize passivity and input strict passivity, as specific cases of dissipativity, for the hybrid dynamical system $\mathcal{G}$ in terms of system functions and the storage function $V(\boldsymbol{x},t)$ via the KYP conditions. The results developed in this section will assume considerable significance in Sec. III to design the hybrid nonlinear passivity-based control schemes in question.

Theorem 1: Consider the hybrid dynamical system $\mathcal{G}$ with $m_{ct}=q_{ct}$, $m_{ds}=q_{ds}$, $\mathcal{D}=\mathbb{R}^n$, $\boldsymbol{U}_{ct}=\mathbb{R}^{m_{ct}}$, $\boldsymbol{Y}_{ct}=\mathbb{R}^{q_{ct}}$, $\boldsymbol{U}_{ds}=\mathbb{R}^{m_{ds}}$, and $\boldsymbol{Y}_{ds}=\mathbb{R}^{q_{ds}}$. Furthermore, assume that the dynamical properties of the system in question evolve periodically over time. If there exist functions $V:\mathbb{R}^n\times\mathbb{R}\to\mathbb{R}$, $\boldsymbol{l}_{ct}:\mathbb{R}^n\times\mathbb{R}\to\mathbb{R}^{p_{ct}}$, $\boldsymbol{l}_{ds}:\mathbb{R}^n\times\mathbb{R}\to\mathbb{R}^{p_{ds}}$, $\boldsymbol{w}_{ct}:\mathbb{R}^n\times\mathbb{R}\to\mathbb{R}^{p_{ct}\times m_{ct}}$, and $\boldsymbol{w}_{ds}:\mathbb{R}^n\times\mathbb{R}\to\mathbb{R}^{p_{ds}\times m_{ds}}$ such that: (I) $V(\boldsymbol{x},t)$ is continuously differentiable and positive definite, (II) $V(\boldsymbol{0},t)=0$, (III) the storage function in the jump manifold is structurally constrained to conform to

$$\begin{aligned}V(\boldsymbol{x}_k^+,t_k^+)&=V(\boldsymbol{f}_{ds}+\boldsymbol{g}_{ds}\boldsymbol{u}_{ds},t_k^+)\\&=V(\boldsymbol{f}_{ds},t_k^+)+\left(\frac{\partial V(\boldsymbol{f}_{ds},t_k^+)}{\partial\boldsymbol{x}}\right)^{\mathrm{T}}\boldsymbol{g}_{ds}\boldsymbol{u}_{ds}(t_k)+\frac{1}{2}\boldsymbol{u}_{ds}^{\mathrm{T}}(t_k)\boldsymbol{g}_{ds}^{\mathrm{T}}\frac{\partial^2V(\boldsymbol{f}_{ds},t_k^+)}{\partial\boldsymbol{x}\partial\boldsymbol{x}^{\mathrm{T}}}\boldsymbol{g}_{ds}\boldsymbol{u}_{ds}(t_k)\end{aligned}\tag{10}$$

for all $\boldsymbol{x}\in\mathbb{R}^n$ and $\boldsymbol{u}_{ds}\in\mathbb{R}^{m_{ds}}$, and (IV) continuous-time and discrete-time equations of the form

$$\frac{\partial V(\boldsymbol{x},t)}{\partial t}+\left(\frac{\partial V(\boldsymbol{x},t)}{\partial\boldsymbol{x}}\right)^{\mathrm{T}}\boldsymbol{f}_{ct}(\boldsymbol{x},t)+\boldsymbol{l}_{ct}^{\mathrm{T}}(\boldsymbol{x},t)\boldsymbol{l}_{ct}(\boldsymbol{x},t)=0\tag{11}$$

$$\frac{1}{2}\left(\frac{\partial V(\boldsymbol{x},t)}{\partial\boldsymbol{x}}\right)^{\mathrm{T}}\boldsymbol{g}_{ct}(\boldsymbol{x},t)-\boldsymbol{h}_{ct}^{\mathrm{T}}(\boldsymbol{x},t)+\boldsymbol{l}_{ct}^{\mathrm{T}}(\boldsymbol{x},t)\boldsymbol{w}_{ct}(\boldsymbol{x},t)=\boldsymbol{0}\tag{12}$$

$$-2\gamma_{ct}\boldsymbol{1}_{m_{ct}\times m_{ct}}+\boldsymbol{j}_{ct}(\boldsymbol{x},t)+\boldsymbol{j}_{ct}^{\mathrm{T}}(\boldsymbol{x},t)-\boldsymbol{w}_{ct}^{\mathrm{T}}(\boldsymbol{x},t)\boldsymbol{w}_{ct}(\boldsymbol{x},t)=\boldsymbol{0}\tag{13}$$

$$V(\boldsymbol{f}_{ds},t_k^+)-V(\boldsymbol{x}_k^-,t_k^-)+\boldsymbol{l}_{ds}^{\mathrm{T}}(\boldsymbol{x}_k,t_k)\boldsymbol{l}_{ds}(\boldsymbol{x}_k,t_k)=0\tag{14}$$

$$\frac{1}{2}\left(\frac{\partial V(\boldsymbol{f}_{ds},t_k^+)}{\partial\boldsymbol{x}}\right)^{\mathrm{T}}\boldsymbol{g}_{ds}-\boldsymbol{h}_{ds}^{\mathrm{T}}(\boldsymbol{x}_k,t_k)+\boldsymbol{l}_{ds}^{\mathrm{T}}(\boldsymbol{x}_k,t_k)\boldsymbol{w}_{ds}(\boldsymbol{x}_k,t_k)=\boldsymbol{0}\tag{15}$$

$$-2\gamma_{ds}\boldsymbol{1}_{m_{ds}\times m_{ds}}+\boldsymbol{j}_{ds}(\boldsymbol{x}_k,t_k)+\boldsymbol{j}_{ds}^{\mathrm{T}}(\boldsymbol{x}_k,t_k)-\frac{1}{2}\boldsymbol{g}_{ds}^{\mathrm{T}}\frac{\partial^2V(\boldsymbol{f}_{ds},t_k^+)}{\partial\boldsymbol{x}\partial\boldsymbol{x}^{\mathrm{T}}}\boldsymbol{g}_{ds}-\boldsymbol{w}_{ds}^{\mathrm{T}}(\boldsymbol{x}_k,t_k)\boldsymbol{w}_{ds}(\boldsymbol{x}_k,t_k)=\boldsymbol{0}\tag{16}$$

are fulfilled for $\gamma_{ct} \geq 0$, $\gamma_{ds} \geq 0$, and all $\boldsymbol{x} \in \mathbb{R}^n$ (wherein $\mathbf{1}$ denotes the identity matrix); the hybrid dynamical system $\mathcal{G}$ is then passive if $\gamma_{ct} = \gamma_{ds} \equiv 0$, and is input strictly passive if $\gamma_{ct} > 0$ and $\gamma_{ds} > 0$.

Proof: Refer to [28].

C. Hybrid Linear Time-varying KYP Conditions

In this section, the KYP conditions developed in the preceding section are specialized to hybrid linear dynamical systems. The resultant linear passivity-related and strict passivity-related KYP conditions can be employed to derive the linear equivalences of the hybrid nonlinear passivity-based control architectures being proposed. Defining $\boldsymbol{x}_{eq} = \mathbf{0}$ as desired operating points for the linearization, the hybrid nonlinear dynamical system represented by Eqs. (1)-(4) can be linearized as below:

$$\dot{\boldsymbol{x}}(t) = \boldsymbol{A}_{ct}(t)\boldsymbol{x} + \boldsymbol{B}_{ct}(t)\boldsymbol{u}_{ct}(t) \ , \ \boldsymbol{x}(\mathbf{0}) = \boldsymbol{x}_0 \qquad t \neq t_k \tag{17}$$

$$\boldsymbol{y}_{ct}(t) = \boldsymbol{C}_{ct}(t)\boldsymbol{x} + \boldsymbol{D}_{ct}(t)\boldsymbol{u}_{ct}(t) \qquad t \neq t_k \tag{18}$$

$$\boldsymbol{x}_k^+ = \boldsymbol{A}_{ds}(t)\boldsymbol{x}_k^- + \boldsymbol{B}_{ds}(t)\boldsymbol{u}_{ds}(t) \qquad t = t_k \tag{19}$$

$$\boldsymbol{y}_{ds}(t) = \boldsymbol{C}_{ds}(t)\boldsymbol{x}_k^- + \boldsymbol{D}_{ds}(t)\boldsymbol{u}_{ds}(t) \qquad t = t_k \tag{20}$$

where $\boldsymbol{A}_{ct} = \mathbf{J}_{\boldsymbol{x}}(\boldsymbol{f}_{ct})\big|_{\boldsymbol{x}=\boldsymbol{x}_{eq}} \in \mathbb{R}^{n\times n}$, $\boldsymbol{B}_{ct} = \boldsymbol{g}_{ct}\big|_{\boldsymbol{x}=\boldsymbol{x}_{eq}} \in \mathbb{R}^{n\times m_{ct}}$, $\boldsymbol{C}_{ct} = \mathbf{J}_{\boldsymbol{x}}(\boldsymbol{h}_{ct})\big|_{\boldsymbol{x}=\boldsymbol{x}_{eq}} \in \mathbb{R}^{q_{ct}\times n}$, $\boldsymbol{D}_{ct} = \boldsymbol{j}_{ct}\big|_{\boldsymbol{x}=\boldsymbol{x}_{eq}} \in \mathbb{R}^{q_{ct}\times m_{ct}}$, $\boldsymbol{A}_{ds} = \mathbf{J}_{\boldsymbol{x}}(\boldsymbol{f}_{ds})\big|_{\boldsymbol{x}=\boldsymbol{x}_{eq}} \in \mathbb{R}^{n\times n}$, $\boldsymbol{B}_{ds} = \boldsymbol{g}_{ds}\big|_{\boldsymbol{x}=\boldsymbol{x}_{eq}} \in \mathbb{R}^{n\times m_{ds}}$, $\boldsymbol{C}_{ds} = \mathbf{J}_{\boldsymbol{x}}(\boldsymbol{h}_{ds})\big|_{\boldsymbol{x}=\boldsymbol{x}_{eq}} \in \mathbb{R}^{q_{ds}\times n}$, and $\boldsymbol{D}_{ds} = \boldsymbol{j}_{ds}\big|_{\boldsymbol{x}=\boldsymbol{x}_{eq}} \in \mathbb{R}^{q_{ds}\times m_{ds}}$ define the system matrices associated with continuous-time and discrete-time subsystems, and $\mathbf{J}_{\boldsymbol{x}}$ denotes the Jacobian matrix with respect to $\boldsymbol{x}$. The KYP conditions characterizing passivity and input strict passivity for hybrid linear dynamical systems can now be presented as follows.

Corollary 1: Consider the linearized hybrid system described by Eqs. (17)-(20) with $m_{ct} = q_{ct}$ and $m_{ds} = q_{ds}$. Furthermore, assume the dynamical properties of the system being considered evolve periodically over time. If there exist matrices $\boldsymbol{P} = \boldsymbol{P}^{\mathrm{T}} \in \mathbb{R}^{n\times n} > \mathbf{0}$ (referred to as *the linear passivity-based gain matrix*), $\boldsymbol{L}_{ct} \in \mathbb{R}^{p_{ct}\times n}$, $\boldsymbol{W}_{ct} \in \mathbb{R}^{p_{ct}\times m_{ct}}$, $\boldsymbol{L}_{ds} \in \mathbb{R}^{p_{ds}\times n}$, and $\boldsymbol{W}_{ds} \in \mathbb{R}^{p_{ds}\times m_{ds}}$ such that continuous-time and discrete-time equations of the form

$$\dot{\boldsymbol{P}}(t) + \boldsymbol{A}_{ct}^{\mathrm{T}}(t)\boldsymbol{P}(t) + \boldsymbol{P}(t)\boldsymbol{A}_{ct}(t) + \boldsymbol{L}_{ct}^{\mathrm{T}}(t)\boldsymbol{L}_{ct}(t) = \mathbf{0} \tag{21}$$

$$\boldsymbol{P}(t)\boldsymbol{B}_{ct}(t) - \boldsymbol{C}_{ct}^{\mathrm{T}}(t) + \boldsymbol{L}_{ct}^{\mathrm{T}}(t)\boldsymbol{W}_{ct}(t) = \mathbf{0} \tag{22}$$

$$\boldsymbol{D}_{ct}(t)+\boldsymbol{D}_{ct}^{\mathrm{T}}(t)-\boldsymbol{W}_{ct}^{\mathrm{T}}(t)\boldsymbol{W}_{ct}(t)=\boldsymbol{0} \tag{23}$$

$$\boldsymbol{A}_{ds}^{\mathrm{T}}(t_k)\boldsymbol{P}(t_k^+)\boldsymbol{A}_{ds}(t_k)-\boldsymbol{P}(t_k^-)+\boldsymbol{L}_{ds}^{\mathrm{T}}(t_k)\boldsymbol{L}_{ds}(t_k)=\boldsymbol{0} \tag{24}$$

$$\boldsymbol{A}_{ds}^{\mathrm{T}}(t_k)\boldsymbol{P}(t_k^+)\boldsymbol{B}_{ds}(t_k)-\boldsymbol{C}_{ds}^{\mathrm{T}}(t_k)+\boldsymbol{L}_{ds}^{\mathrm{T}}(t_k)\boldsymbol{W}_{ds}(t_k)=\boldsymbol{0} \tag{25}$$

$$\boldsymbol{D}_{ds}(t_k)+\boldsymbol{D}_{ds}^{\mathrm{T}}(t_k)-\boldsymbol{B}_{ds}^{\mathrm{T}}(t_k)\boldsymbol{P}(t_k^+)\boldsymbol{B}_{ds}(t_k)-\boldsymbol{W}_{ds}^{\mathrm{T}}(t_k)\boldsymbol{W}_{ds}(t_k)=\boldsymbol{0} \tag{26}$$

are fulfilled for all $\boldsymbol{x}\in\mathbb{R}^n$; the linearized hybrid system is then passive.

Proof: The result is a direct consequence of theorem 1 by setting $\gamma_{ct}=0$, $\gamma_{ds}=0$, $V(\boldsymbol{x},t)=\boldsymbol{x}^{\mathrm{T}}\boldsymbol{P}(t)\boldsymbol{x}$, $\boldsymbol{f}_{ct}=\boldsymbol{A}_{ct}\boldsymbol{x}$, $\boldsymbol{g}_{ct}=\boldsymbol{B}_{ct}$, $\boldsymbol{h}_{ct}=\boldsymbol{C}_{ct}\boldsymbol{x}$, $\boldsymbol{j}_{ct}=\boldsymbol{D}_{ct}$, $\boldsymbol{f}_{ds}=\boldsymbol{A}_{ds}\boldsymbol{x}_k^-$, $\boldsymbol{g}_{ds}=\boldsymbol{B}_{ds}$, $\boldsymbol{h}_{ds}=\boldsymbol{C}_{ds}\boldsymbol{x}_k^-$, $\boldsymbol{j}_{ds}=\boldsymbol{D}_{ds}$, $\boldsymbol{l}_{ct}=\boldsymbol{L}_{ct}\boldsymbol{x}$, $\boldsymbol{w}_{ct}=\boldsymbol{W}_{ct}$, $\boldsymbol{l}_{ds}=\boldsymbol{L}_{ds}\boldsymbol{x}$, and $\boldsymbol{w}_{ds}=\boldsymbol{W}_{ds}$.

Corollary 2: Consider the linearized hybrid system given by Eqs. (17)-(20) with $m_{ct}=q_{ct}$ and $m_{ds}=q_{ds}$. If there exist matrices $\boldsymbol{\mathcal{P}}=\boldsymbol{\mathcal{P}}^{\mathrm{T}}\in\mathbb{R}^{n\times n}>\boldsymbol{0}$ (referred to as *the linear strict passivity-based gain matrix*), $\boldsymbol{\mathcal{L}}_{ct}\in\mathbb{R}^{p_{ct}\times n}$, $\boldsymbol{\mathcal{W}}_{ct}\in\mathbb{R}^{p_{ct}\times m_{ct}}$, $\boldsymbol{\mathcal{L}}_{ds}\in\mathbb{R}^{p_{ds}\times n}$, and $\boldsymbol{\mathcal{W}}_{ds}\in\mathbb{R}^{p_{ds}\times m_{ds}}$ such that continuous-time and discrete-time equations of the form

$$\dot{\boldsymbol{\mathcal{P}}}(t)+\boldsymbol{A}_{ct}^{\mathrm{T}}(t)\boldsymbol{\mathcal{P}}(t)+\boldsymbol{\mathcal{P}}(t)\boldsymbol{A}_{ct}(t)+\boldsymbol{\mathcal{L}}_{ct}^{\mathrm{T}}(t)\boldsymbol{\mathcal{L}}_{ct}(t)=\boldsymbol{0} \tag{27}$$

$$\boldsymbol{\mathcal{P}}(t)\boldsymbol{B}_{ct}(t)-\boldsymbol{C}_{ct}^{\mathrm{T}}(t)+\boldsymbol{\mathcal{L}}_{ct}^{\mathrm{T}}(t)\boldsymbol{\mathcal{W}}_{ct}(t)=\boldsymbol{0} \tag{28}$$

$$-2\gamma_{ct}\boldsymbol{1}_{m_{ct}\times m_{ct}}+\boldsymbol{D}_{ct}(t)+\boldsymbol{D}_{ct}^{\mathrm{T}}(t)-\boldsymbol{\mathcal{W}}_{ct}^{\mathrm{T}}(t)\boldsymbol{\mathcal{W}}_{ct}(t)=\boldsymbol{0} \tag{29}$$

$$\boldsymbol{A}_{ds}^{\mathrm{T}}(t_k)\boldsymbol{\mathcal{P}}(t_k^+)\boldsymbol{A}_{ds}(t_k)-\boldsymbol{\mathcal{P}}(t_k^-)+\boldsymbol{\mathcal{L}}_{ds}^{\mathrm{T}}(t_k)\boldsymbol{\mathcal{L}}_{ds}(t_k)=\boldsymbol{0} \tag{30}$$

$$\boldsymbol{A}_{ds}^{\mathrm{T}}(t_k)\boldsymbol{\mathcal{P}}(t_k^+)\boldsymbol{B}_{ds}(t_k)-\boldsymbol{C}_{ds}^{\mathrm{T}}(t_k)+\boldsymbol{\mathcal{L}}_{ds}^{\mathrm{T}}(t_k)\boldsymbol{\mathcal{W}}_{ds}(t_k)=\boldsymbol{0} \tag{31}$$

$$-2\gamma_{ds}\boldsymbol{1}_{m_{ds}\times m_{ds}}+\boldsymbol{D}_{ds}(t_k)+\boldsymbol{D}_{ds}^{\mathrm{T}}(t_k)-\boldsymbol{B}_{ds}^{\mathrm{T}}(t_k)\boldsymbol{\mathcal{P}}(t_k^+)\boldsymbol{B}_{ds}(t_k)-\boldsymbol{\mathcal{W}}_{ds}^{\mathrm{T}}(t_k)\boldsymbol{\mathcal{W}}_{ds}(t_k)=\boldsymbol{0} \tag{32}$$

are met for $\gamma_{ct}>0$, $\gamma_{ds}>0$, and all $\boldsymbol{x}\in\mathbb{R}^n$; the linearized hybrid system is then input strictly passive.

Proof: The result is a direct consequence of theorem 1 by setting $\gamma_{ct}\neq 0$, $\gamma_{ds}\neq 0$, $V(\boldsymbol{x},t)=\boldsymbol{x}^{\mathrm{T}}\boldsymbol{\mathcal{P}}(t)\boldsymbol{x}$, $\boldsymbol{f}_{ct}=\boldsymbol{A}_{ct}\boldsymbol{x}$, $\boldsymbol{g}_{ct}=\boldsymbol{B}_{ct}$, $\boldsymbol{h}_{ct}=\boldsymbol{C}_{ct}\boldsymbol{x}$, $\boldsymbol{j}_{ct}=\boldsymbol{D}_{ct}$, $\boldsymbol{f}_{ds}=\boldsymbol{A}_{ds}\boldsymbol{x}_k^-$, $\boldsymbol{g}_{ds}=\boldsymbol{B}_{ds}$, $\boldsymbol{h}_{ds}=\boldsymbol{C}_{ds}\boldsymbol{x}_k^-$, $\boldsymbol{j}_{ds}=\boldsymbol{D}_{ds}$, $\boldsymbol{l}_{ct}=\boldsymbol{\mathcal{L}}_{ct}\boldsymbol{x}$, $\boldsymbol{w}_{ct}=\boldsymbol{\mathcal{W}}_{ct}$, $\boldsymbol{l}_{ds}=\boldsymbol{\mathcal{L}}_{ds}\boldsymbol{x}$, and $\boldsymbol{w}_{ds}=\boldsymbol{\mathcal{W}}_{ds}$.

D. Feedback Interconnection of Hybrid Dissipative Systems

Placing the passivity theorem as a solid foundation, this section aims to discuss the feedback interconnection of hybrid dissipative dynamical systems so as to construct stable closed-loop dynamics. In accordance with the

passivity theorem, the negative feedback interconnection of a passive system and an input strictly passive system is input-output stable. Figure 1 shows a schematic representation of a closed-loop system established by the negative feedback interconnection of a hybrid plant $\mathcal{G}$ and a hybrid controller $\mathcal{H}$ wherein $(\boldsymbol{d}_{ct}, \boldsymbol{d}_{ds})$ denotes hybrid external disturbances; $(\boldsymbol{u}_{ct}, \boldsymbol{u}_{ds,k})$ is the hybrid input of the plant to be controlled wherein $\boldsymbol{u}_{ds,k} \triangleq \boldsymbol{u}_{ds}\left(\boldsymbol{x}(t_k), t_k\right)$; $(\widehat{\boldsymbol{u}}_{ct}, \widehat{\boldsymbol{u}}_{ds,k})$ represents the hybrid input of the controller with $\widehat{\boldsymbol{u}}_{ds,k} \triangleq \widehat{\boldsymbol{u}}_{ds}\left(\widehat{\boldsymbol{x}}(t_k), t_k\right)$, which is equal to the hybrid output of the plant $(\boldsymbol{y}_{ct}, \boldsymbol{y}_{ds,k})$ where $\boldsymbol{y}_{ds,k} \triangleq \boldsymbol{y}_{ds}\left(\boldsymbol{x}(t_k), t_k\right)$; and $(\widehat{\boldsymbol{y}}_{ct}, \widehat{\boldsymbol{y}}_{ds,k})$ specifies the hybrid output of the controller with $\widehat{\boldsymbol{y}}_{ds,k} \triangleq \widehat{\boldsymbol{y}}_{ds}\left(\widehat{\boldsymbol{x}}(t_k), t_k\right)$. In view of the passivity theorem, three essential ingredients can therefore be combined to accomplish the main objective of constructing stable closed-loop dynamics: a passive plant, an input strictly passive controller, and a negative feedback interconnection between the resultant plant and controller.

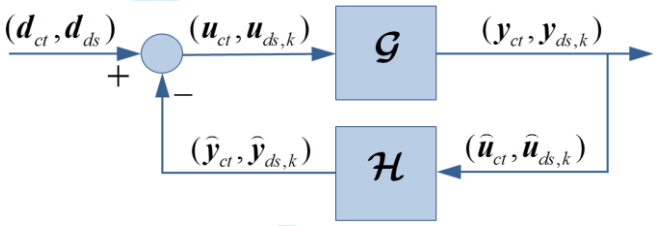

Fig. 1. Schematic representation of closed-loop system composed of hybrid plant $\mathcal{G}$ and hybrid controller $\mathcal{H}$

III. Passivity-based Control Approach

The results presented in Secs. II.B (theorem 1) and II.C (corollary 2) are employed in this section to develop two passivity-based control design frameworks for nonlinear systems with heterogeneous dynamics whose dynamical properties evolve over time. In both architectures, a three-step control design procedure based upon the passivity theorem is followed to attain the main objective, that is, to render the closed-loop system stable. In this regard, the hybrid output dynamics of the plant are first determined in a judicious manner to fulfill the passivity specifications through the passivity-related KYP conditions given by Eqs. (11)-(16) with $\gamma_{ct} = \gamma_{ds} \equiv 0$. By utilizing compensators of static and dynamic structures, a hybrid controller, the input of which is directly fed by the plant's output, is then designed to meet the input strict passivity requirements via the KYP conditions associated with strict passivity. The input-output stability of the closed-loop system is finally established by a negative feedback interconnection between the (passive) plant $\mathcal{G}$ and the (input strictly passive) controller $\mathcal{H}$ (See Fig. 1).

To pursue the main objective, Eqs. (11) and (14) must first be solved simultaneously for $V(\boldsymbol{x},t)$ in an interacting manner. The hybrid output of the plant can then be determined in terms of $V(\boldsymbol{x},t)$ through the remaining conditions. These equations are, however, difficult to solve in general, thereby necessitating approximation techniques. Two numerical methods are therefore employed in the following sections to approximate Eqs. (11) and (14). The Galerkin spectral method [29] is utilized in Sec. III.A to approximate the storage function involved in the differential passivity-related KYP equation [Eq. (11)], thereby computing the passivity-based control gains between impulsive events. By making use of the spectral collocation method [30], the difference passivity-related KYP equation [Eq. (14)] is then approximated in Sec. III.B to find the passivity-based control gain vector at impulsive instants.

A. Numerical Solution to Passivity-related KYP$_{ct}$ Conditions

Applying the Galerkin spectral method to the differential passivity-related KYP condition, a set of differential equations is derived in this section to compute the passivity-based control gains between impulsive instants. These time-varying coefficients are subsequently used to construct the continuous-time output of interest for the plant. The basic idea underlying Galerkin's spectral approach is to assume that the solution to Eq. (11) can be expressed as an infinite sum of known basis functions. In addition, in order for the Galerkin method to be applicable, the problem must be placed in a suitable inner product space such that the projection is well-defined in terms of *n*-dimensional integrations [29]. The approximation is thus restricted to a closed and bounded set in $\mathcal{D}$, namely a compact set $\boldsymbol{\Omega}$, which defines the bounded domain of the state space of interest. Therefore, it is first assumed that the storage function involved in Eq. (11) can be discretized by an infinite series of prescribed state-dependent basis functions, which are continuous and defined everywhere on $\boldsymbol{\Omega}$, and unknown coefficients with time-dependency as below:

$$V(\boldsymbol{x},t) \coloneqq \sum_{j=1}^{\infty} c_j(t)\,\phi_j(\boldsymbol{x}) \tag{33}$$

Nevertheless, from a practical perspective, using an infinite number of terms in the discretization is impossible; the approximation process for $V(\boldsymbol{x},t)$ is therefore carried one step further by considering a truncated version of the infinite series (i.e. the first *N* terms):

$$V_N(\boldsymbol{x},t) \coloneqq \sum_{j=1}^{N} c_j(t)\,\phi_j(\boldsymbol{x}) = \boldsymbol{\Phi}_N^{\mathrm{T}}(\boldsymbol{x})\boldsymbol{\mathcal{C}}_N(t) \tag{34}$$

wherein $\boldsymbol{\Phi}_N(\boldsymbol{x}) = [\phi_1, ..., \phi_N]^{\mathrm{T}}$ represents a prescribed state-dependent set of basis functions, $\boldsymbol{\mathcal{C}}_N(t) = [c_1, ..., c_N]^{\mathrm{T}}$ specifies the corresponding collection of unknown time-dependent coefficients, and *N* denotes the number of basis elements, i.e. the order of approximation. The approximation sequence then proceeds with substituting (34) into Eq. (11) which, in turn, leads to an error function due primarily to approximating the storage function with $V_N(\boldsymbol{x}, t)$. Following the Galerkin spectral method, the unknown coefficients, $\boldsymbol{\mathcal{C}}_N(t)$, are therefore determined such that the resulting error is minimized. To this end, the error function is projected onto the same basis functions retained in the truncated series (i.e. the linear finite basis spanned by $\{\phi_j\}_1^N$) and the outcome is set equal to zero in order to obtain *N* simultaneous equations in *N* unknowns:

$$\left\langle \underset{Passivity}{\mathrm{KYP}_{ct}}\left(\sum_{j=1}^{N} c_j(t)\,\phi_j(\boldsymbol{x}) \right), \boldsymbol{\Phi}_N(\boldsymbol{x}) \right\rangle_{\boldsymbol{\Omega}} = \mathbf{0} \tag{35}$$

wherein the projection operator is the inner product $\langle (\cdot), \phi_i(\boldsymbol{x}) \rangle_{\boldsymbol{\Omega}} \triangleq \int_{\boldsymbol{\Omega}} (\cdot)\phi_i(\boldsymbol{x}) d\boldsymbol{x}$ computed over a closed and bounded set $\boldsymbol{\Omega}$. Equation (35) represents the Galerkin-based projection of the differential passivity-related KYP equation [Eq. (11)] in a compact form, which can be expanded as follows:

$$\langle \boldsymbol{\Phi}_N, \boldsymbol{\Phi}_N \rangle_{\boldsymbol{\Omega}} \dot{\boldsymbol{\mathcal{C}}}_N(t) + \langle \mathbf{J}_{\boldsymbol{x}}(\boldsymbol{\Phi}_N)\, \boldsymbol{f}_{ct}, \boldsymbol{\Phi}_N \rangle_{\boldsymbol{\Omega}} \boldsymbol{\mathcal{C}}_N(t) + \langle \boldsymbol{l}_{ct}^{\mathrm{T}} \boldsymbol{l}_{ct}, \boldsymbol{\Phi}_N \rangle_{\boldsymbol{\Omega}} = \mathbf{0} \tag{36}$$

Considering $\boldsymbol{l}_{ct}(\boldsymbol{x}, t)$ as a design parameter to be appropriately selected by the user, the following set of ordinary differential equations, known as *the continuous-time passivity-based control gain equations*, needs therefore to be integrated backward in time in order to compute $\boldsymbol{\mathcal{C}}_N(t)$ between impulsive instants:

$$\dot{\boldsymbol{\mathcal{C}}}_N(t) + \boldsymbol{\mathcal{M}}(t)\boldsymbol{\mathcal{C}}_N(t) + \boldsymbol{\beta}(t) = \mathbf{0} \quad , \quad \boldsymbol{\mathcal{C}}_N(t_{\mathrm{f}}) = \boldsymbol{\mathcal{C}}_{\mathrm{f}} \tag{37}$$

where $\boldsymbol{\mathcal{C}}_{\mathrm{f}}$ denote the boundary conditions at the terminal time defined by the user as a design parameter, and

$$\begin{aligned} \boldsymbol{\mathcal{M}}(t) &= \langle \boldsymbol{\Phi}_N, \boldsymbol{\Phi}_N \rangle_{\boldsymbol{\Omega}}^{-1} \langle \mathbf{J}_{\boldsymbol{x}}(\boldsymbol{\Phi}_N)\, \boldsymbol{f}_{ct}, \boldsymbol{\Phi}_N \rangle_{\boldsymbol{\Omega}} \\ \boldsymbol{\beta}(t) &= \langle \boldsymbol{\Phi}_N, \boldsymbol{\Phi}_N \rangle_{\boldsymbol{\Omega}}^{-1} \langle \boldsymbol{l}_{ct}^{\mathrm{T}} \boldsymbol{l}_{ct}, \boldsymbol{\Phi}_N \rangle_{\boldsymbol{\Omega}} \end{aligned} \tag{38}$$

Once the passivity-based control gains, $\boldsymbol{\mathcal{C}}_N(t)$, are computed via backward integration of Eq. (37), the continuous-time output of interest, $\boldsymbol{y}_{ct}$, can be determined through Eqs. (12) and (13) with $\gamma_{ct} = 0$. To this end, the

simplifying assumptions of $\boldsymbol{w}_{ct}(\boldsymbol{x},t)\equiv\boldsymbol{0}$ and $\boldsymbol{j}_{ct}(\boldsymbol{x},t)=\boldsymbol{j}_{ct}^{\mathrm{T}}(\boldsymbol{x},t)$ are made to limit the design space. As a consequence, Eq. (13) leads to $\boldsymbol{j}_{ct}(\boldsymbol{x},t)=\boldsymbol{0}$, and the continuous-time output of the plant, which satisfies the passivity specifications in the continuous-time subsystem, is ultimately obtained by:

$$\begin{aligned}\boldsymbol{y}_{ct}(\boldsymbol{x},t)&=\boldsymbol{h}_{ct}(\boldsymbol{x},t)+\boldsymbol{j}_{ct}(\boldsymbol{x},t)\boldsymbol{u}_{ct}(t)\\&=\boldsymbol{h}_{ct}(\boldsymbol{x},t)=\frac{1}{2}\boldsymbol{g}_{ct}^{\mathrm{T}}(\boldsymbol{x},t)\mathbf{J}_{\boldsymbol{x}}^{\mathrm{T}}\left(\boldsymbol{\Phi}_N(\boldsymbol{x})\right)\boldsymbol{\mathcal{C}}_N(t)\end{aligned}\tag{39}$$

Refer to Section V for a detailed discussion on how to select basis functions.

B. Numerical Solution to Passivity-related KYP$_{ds}$ Conditions

With the continuous-time passivity-based control gain equations [Eq. (37)] thus derived, a set of algebraic equations is developed in this section to be solved for the unknown time-dependent coefficients vector when an impulse occurs. In this regard, the spectral collocation method is utilized to approximate the difference passivity-related KYP equation [Eq. (14)], thereby computing the passivity-based control gain vector at impulsive instants. The main idea behind the collocation strategy is to project Eq. (14) onto a discrete basis to produce as many equations as required for the unknowns. This is analogous to the Galerkin spectral method where the error function resulting from approximating the storage function is projected onto a set of basis elements to obtain *N* simultaneous equations in *N* unknowns.

Preparatory to deriving the discrete-time counterpart of passivity-based control gain equations, the truncated version of the discretized storage function [Eq. (34)] is substituted into Eq. (14) to formulate the following set of algebraic equations at each jump instant, $t=t_k$:

$$\boldsymbol{\Phi}_N^{\mathrm{T}}(\boldsymbol{x})\big|_{\boldsymbol{x}=\boldsymbol{f}_{ds}}\boldsymbol{\mathcal{C}}_N(t_k^+)-\boldsymbol{\Phi}_N^{\mathrm{T}}(\boldsymbol{x}_k^-)\boldsymbol{\mathcal{C}}_N(t_k^-)+\boldsymbol{l}_{ds}^{\mathrm{T}}(\boldsymbol{x}_k^-,t_k^-)\boldsymbol{l}_{ds}(\boldsymbol{x}_k^-,t_k^-)=0\tag{40}$$

Having $\boldsymbol{\mathcal{C}}_N(t_k^+)$ available from the backward integration of Eq. (37), $\boldsymbol{\mathcal{C}}_N(t_k^-)$ can thus be computed through the preceding set of equations. However, the state knowledge at $t=t_k^-$, $\boldsymbol{x}_k^-$, is required to reach this objective, which, in consequence, provides a new challenge. Aiming to rise to this challenge, $\boldsymbol{x}_k^-$ is collocated with a suitable set of points, $\bar{\boldsymbol{x}}=\underset{m}{\mathrm{row}}\left\{\bar{\boldsymbol{x}}_m\right\}$ wherein $\bar{\boldsymbol{x}}_m\in\mathbb{R}^n$ and $m=1,\ldots,N$, at each jump instant to obtain *N* equations in *N* unknowns. The following set of algebraic equations, termed as *the discrete-time passivity-based control gain equations*, must therefore be solved for $\boldsymbol{\mathcal{C}}_N(t_k^-)$ every time an impulse is applied:

$$\boldsymbol{\mathcal{C}}_N(t_k^-) = \left(\boldsymbol{\Psi}_k(\bar{\boldsymbol{x}})\right)^{-1}\left[\boldsymbol{\Upsilon}_k(\bar{\boldsymbol{x}}, t_k^-) + \mathbf{Z}_k(\bar{\boldsymbol{x}}, t_k^-)\boldsymbol{\mathcal{C}}_N(t_k^+)\right] \tag{41}$$

where

$$\begin{aligned}
\boldsymbol{\Upsilon}_k(\bar{\boldsymbol{x}}, t_k^-) &= \underset{m}{\text{column}}\left\{\boldsymbol{l}_{ds}^{\mathrm{T}}(\bar{\boldsymbol{x}}_m, t_k^-)\boldsymbol{l}_{ds}(\bar{\boldsymbol{x}}_m, t_k^-)\right\} \\
\boldsymbol{\Psi}_k(\bar{\boldsymbol{x}}) &= \underset{m,j}{\text{matrix}}\left\{\phi_j(\bar{\boldsymbol{x}}_m)\right\} \\
\mathbf{Z}_k(\bar{\boldsymbol{x}}, t_k^-) &= \underset{m,j}{\text{matrix}}\left\{\phi_j(\boldsymbol{x})\big|_{\boldsymbol{x}=\boldsymbol{f}_{ds}(\bar{\boldsymbol{x}}_m, t_k^-)}\right\}
\end{aligned} \tag{42}$$

wherein $\boldsymbol{l}_{ds}(\boldsymbol{x}_k^-, t_k^-)$ is assumed to act as a design parameter to be appropriately chosen by the user.

With the control gain vector thus computed at each impulsive instant, the discrete-time output of interest, $\boldsymbol{y}_{ds,k}$, at each jump can therefore be determined through Eqs. (15) and (16) with $\gamma_{ds} = 0$. In this regard, as to the continuous-time subsystem, simplifying assumptions in the form of $\boldsymbol{w}_{ds}(\boldsymbol{x}, t) \equiv \mathbf{0}$ and $\boldsymbol{j}_{ds}(\boldsymbol{x}, t) = \boldsymbol{j}_{ds}^{\mathrm{T}}(\boldsymbol{x}, t)$ are made with the purpose of limiting the design space, and $\boldsymbol{h}_{ds}$ and $\boldsymbol{j}_{ds}$ are accordingly obtained as follows:

$$\boldsymbol{h}_{ds}(\boldsymbol{x}_k^-, t_k) = \frac{1}{2}\boldsymbol{g}_{ds}^{\mathrm{T}}(\boldsymbol{x}_k^-, t_k)\,\mathbf{J}_{\boldsymbol{x}}^{\mathrm{T}}\left(\boldsymbol{\Phi}_N(\boldsymbol{x})\right)\big|_{\boldsymbol{x}=\boldsymbol{f}_{ds}}\,\boldsymbol{\mathcal{C}}_N(t_k^+) \tag{43}$$

$$\boldsymbol{j}_{ds}(\boldsymbol{x}_k^-, t_k) = \frac{1}{4}\boldsymbol{g}_{ds}^{\mathrm{T}}(\boldsymbol{x}_k^-, t_k)\sum_{j=1}^{N} c_j(t_k^+)\,\mathbf{H}_{\boldsymbol{x}}\left(\phi_j(\boldsymbol{x})\right)\big|_{\boldsymbol{x}=\boldsymbol{f}_{ds}}\,\boldsymbol{g}_{ds}(\boldsymbol{x}_k^-, t_k) \tag{44}$$

where $\mathbf{H}_{\boldsymbol{x}}$ is the Hessian matrix with respect to $\boldsymbol{x}$. The discrete-time output of the plant, the dynamics of which fulfill the passivity specifications in the discrete-time subsystem, can therefore be calculated by:

$$\begin{aligned}
\boldsymbol{y}_{ds,k} &= \boldsymbol{h}_{ds}(\boldsymbol{x}_k^-, t_k) + \boldsymbol{j}_{ds}(\boldsymbol{x}_k^-, t_k)\boldsymbol{u}_{ds,k} \\
&= \frac{1}{2}\boldsymbol{g}_{ds}^{\mathrm{T}}\,\mathbf{J}_{\boldsymbol{x}}^{\mathrm{T}}\left(\boldsymbol{\Phi}_N(\boldsymbol{x})\right)\big|_{\boldsymbol{x}=\boldsymbol{f}_{ds}}\,\boldsymbol{\mathcal{C}}_N(t_k^+) + \frac{1}{4}\boldsymbol{g}_{ds}^{\mathrm{T}}\sum_{j=1}^{N} c_j(t_k^+)\,\mathbf{H}_{\boldsymbol{x}}\left(\phi_j(\boldsymbol{x})\right)\big|_{\boldsymbol{x}=\boldsymbol{f}_{ds}}\,\boldsymbol{g}_{ds}\boldsymbol{u}_{ds,k}
\end{aligned} \tag{45}$$

C. Passivity Specifications for Hybrid Plant

Armed with the continuous-time and discrete-time passivity-based control gain equations, Eqs. (37) and (41) respectively, the desired hybrid nonlinear passivity-based control gain vector can be obtained at each time instant via solving the following set of equations for $\boldsymbol{\mathcal{C}}_N(t)$:

$$\begin{cases}
\dot{\boldsymbol{\mathcal{C}}}_N(t) + \boldsymbol{\mathcal{M}}(t)\boldsymbol{\mathcal{C}}_N(t) + \boldsymbol{\beta}(t) = \mathbf{0}\ ,\ \boldsymbol{\mathcal{C}}_N(t_{\mathrm{f}}) = \boldsymbol{\mathcal{C}}_{\mathrm{f}} & [\text{See Eq.(38)}] \quad t \neq t_k \\
\boldsymbol{\mathcal{C}}_N(t_k^-) = \left(\boldsymbol{\Psi}_k(\bar{\boldsymbol{x}})\right)^{-1}\left[\boldsymbol{\Upsilon}_k(\bar{\boldsymbol{x}}, t_k^-) + \mathbf{Z}_k(\bar{\boldsymbol{x}}, t_k^-)\boldsymbol{\mathcal{C}}_N(t_k^+)\right] & [\text{See Eq.(42)}] \quad t = t_k
\end{cases} \tag{46}$$

Beginning with the boundary conditions at the terminal time $\mathcal{C}_{\mathrm{f}}$, the continuous-time set of equations are first integrated backward in time to compute $\mathcal{C}_N(t)$ between impulsive instants. Once a specific criterion is met, an impulse is induced in the solution at $t = t_k$ through exciting the discrete-time control gain equations fed by $\mathcal{C}_N(t_k^+)$ and, in consequence, the continuous evolution of $\mathcal{C}_N(t)$ is instantaneously switched to a quantum leap occurring in a jump manifold. $\mathcal{C}_N(t_k^-)$ computed at the jump instant is subsequently used as a new set of terminal conditions for the continuous-time control gain equations to be integrated backward from t_k^- to t_{k-1}^+. Exhibiting continuous evolutions and instantaneous jumps in appropriate manifolds, the solution maintains this sequence until time zero is reached.

Once the hybrid nonlinear passivity-based control gain vector is computed at each time instant via solving *the hybrid passivity-based control gain equations* [Eq. (46)], the hybrid output of the plant, the heterogeneous dynamics of which guarantee a passive hybrid map from input to output, can thus be formulated as an interacting pair of continuous-time and discrete-time outputs:

$$\begin{cases} \boldsymbol{y}_{ct}(\boldsymbol{x},t) = \dfrac{1}{2}\boldsymbol{g}_{ct}^{\mathrm{T}}\mathbf{J}_{\boldsymbol{x}}^{\mathrm{T}}\left(\boldsymbol{\Phi}_N(\boldsymbol{x})\right)\mathcal{C}_N(t) & t \neq t_k \\ \boldsymbol{y}_{ds,k} = \dfrac{1}{2}\boldsymbol{g}_{ds}^{\mathrm{T}}\mathbf{J}_{\boldsymbol{x}}^{\mathrm{T}}\left(\boldsymbol{\Phi}_N(\boldsymbol{x})\right)\Big|_{\boldsymbol{x}=\boldsymbol{f}_{ds}}\mathcal{C}_N(t_k^+) + \dfrac{1}{4}\boldsymbol{g}_{ds}^{\mathrm{T}}\sum_{j=1}^{N}c_j(t_k^+)\mathbf{H}_{\boldsymbol{x}}\left(\phi_j(\boldsymbol{x})\right)\Big|_{\boldsymbol{x}=\boldsymbol{f}_{ds}}\boldsymbol{g}_{ds}\boldsymbol{u}_{ds,k} & t = t_k \end{cases} \tag{47}$$

With the hybrid output of interest coming directly from the hybrid passivity-related KYP conditions [Eqs. (11)-(16) with $\gamma_{ct} = \gamma_{ds} \equiv 0$] thus determined, a hybrid controller capable of meeting the input strict passivity requirements remains to be designed. With the passivity theorem in mind, two distinct structures are employed in the following sections to design the desired hybrid nonlinear controller: a static compensator, which serves to provide proportional output feedback with constant positive gains in each continuous-time and discrete-time subsystem; and a dynamic compensator, the state of which evolves both continuously and discontinuously on appropriate manifolds as time elapses. In both architectures, external disturbances are assumed to be sufficiently small, i.e. $(\boldsymbol{d}_{ct}, \boldsymbol{d}_{ds}) \cong (\mathbf{0}, \mathbf{0})$, and, in consequence, the hybrid output of the controller, $(\hat{\boldsymbol{y}}_{ct}, \hat{\boldsymbol{y}}_{ds,k})$, with negative sign is directly fed back to the plant as its hybrid input (See Fig. 1).

D. Feedback Interconnection via Static Compensator

In the first approach, a hybrid static controller in the form of a hybrid proportional output feedback compensator with constant positive gains, $\mathcal{H} \triangleq (\boldsymbol{K}_{ct}, \boldsymbol{K}_{ds})$ where $\boldsymbol{K}_{ct} = \boldsymbol{K}_{ct}^{\mathrm{T}} > \mathbf{0}$ and $\boldsymbol{K}_{ds} = \boldsymbol{K}_{ds}^{\mathrm{T}} > \mathbf{0}$, is employed to construct the

negative feedback interconnection required for establishing the input-output stability properties of the closed-loop dynamics as follows (See Fig. 1):

$$\boldsymbol{u}_{ct}(\boldsymbol{x},t) = -\hat{\boldsymbol{y}}_{ct} = -\boldsymbol{K}_{ct}\hat{\boldsymbol{u}}_{ct} = -\boldsymbol{K}_{ct}\boldsymbol{y}_{ct}(\boldsymbol{x},t) \qquad t \neq t_k \tag{48}$$

$$\boldsymbol{u}_{ds,k} = -\hat{\boldsymbol{y}}_{ds,k} = -\boldsymbol{K}_{ds}\hat{\boldsymbol{u}}_{ds,k} = -\boldsymbol{K}_{ds}\boldsymbol{y}_{ds,k} \qquad t = t_k \tag{49}$$

Since the proposed static compensator benefits inherently from input strict passivity properties, provided that $\boldsymbol{K}_{ct} = \boldsymbol{K}_{ct}^{\mathrm{T}} > \boldsymbol{0}$ and $\boldsymbol{K}_{ds} = \boldsymbol{K}_{ds}^{\mathrm{T}} > \boldsymbol{0}$, there is no necessity to use the corresponding strict passivity-related KYP conditions. In this regard, the eigendecomposition of the proportional gain matrix can be used to show the strict passivity characteristics of the static compensator. The desired hybrid nonlinear passivity-based control law can therefore be formulated by substituting $(\boldsymbol{y}_{ct}, \boldsymbol{y}_{ds,k})$ [given by Eq. (47)] into Eqs. (48) and (49) as below:

$$\begin{cases} \boldsymbol{u}_{ct}(\boldsymbol{x},t) = -\dfrac{1}{2}\boldsymbol{K}_{ct}\boldsymbol{g}_{ct}^{\mathrm{T}}\mathbf{J}_{\boldsymbol{x}}^{\mathrm{T}}\left(\boldsymbol{\Phi}_N(\boldsymbol{x})\right)\boldsymbol{\mathcal{C}}_N(t) & t \neq t_k \\ \boldsymbol{u}_{ds,k} = -\dfrac{1}{2}\left(\mathbf{1}_{m_{ds}\times m_{ds}} + \dfrac{1}{4}\boldsymbol{K}_{ds}\boldsymbol{g}_{ds}^{\mathrm{T}}\sum_{j=1}^{N} c_j(t_k^+)\mathbf{H}_{\boldsymbol{x}}\left(\phi_j(\boldsymbol{x})\right)\Big|_{\boldsymbol{x}=\boldsymbol{f}_{ds}}\boldsymbol{g}_{ds}\right)^{-1}\boldsymbol{K}_{ds}\boldsymbol{g}_{ds}^{\mathrm{T}}\,\mathbf{J}_{\boldsymbol{x}}^{\mathrm{T}}\left(\boldsymbol{\Phi}_N(\boldsymbol{x})\right)\Big|_{\boldsymbol{x}=\boldsymbol{f}_{ds}}\boldsymbol{\mathcal{C}}_N(t_k^+) & t = t_k \end{cases} \tag{50}$$

The negative feedback interconnection of the plant, which is guaranteed to be passive with $(\boldsymbol{y}_{ct}, \boldsymbol{y}_{ds,k})$ computed by Eq. (47), and the controller in the form of a static compensator, which is inherently strictly passive, is therefore input-output stable as per the passivity theorem.

E. Feedback Interconnection via Dynamic Compensator

Aiming to enhance the control authority and to filter out sensor noise, which in turn contributes significantly to the first objective, a compensator of a dynamic nature is adopted in this section to be interconnected with the passive plant through a negative feedback. The idea of employing a dynamic compensator in a feedback loop has origins in Ref. [31] where, in accordance with the positive real design procedure, the continuous-time linear time-invariant (LTI) KYP conditions were used to develop an embedded control architecture involving a strictly positive (continuous-time) LTI dynamic compensator in order to stabilize large-scale space structures. Complementing the aforementioned continuous-time dynamics with discrete-time events occurring at an appropriate sequence of instants together with endowing the resultant system with a time-dependent character, this paper proposes a time-varying control-affine structure involving an interacting pair of continuous-time and discrete-time dynamics as the dynamic compensator in question, $\mathcal{H}$, as follows:

$$\dot{\hat{\boldsymbol{x}}}(t) = \hat{\boldsymbol{A}}_{ct}(t)\hat{\boldsymbol{x}} + \hat{\boldsymbol{B}}_{ct}(t)\hat{\boldsymbol{u}}_{ct}(t)\ ,\ \hat{\boldsymbol{x}}(\boldsymbol{0}) = \hat{\boldsymbol{x}}_0 \qquad t \neq t_k \tag{51}$$

$$\hat{\boldsymbol{y}}_{ct}(t) = \hat{\boldsymbol{C}}_{ct}(t)\hat{\boldsymbol{x}} + \hat{\boldsymbol{D}}_{ct}(t)\hat{\boldsymbol{u}}_{ct}(t) \qquad t \neq t_k \tag{52}$$

$$\hat{\boldsymbol{x}}_k^+ = \hat{\boldsymbol{A}}_{ds}(t)\hat{\boldsymbol{x}}_k^- + \hat{\boldsymbol{B}}_{ds}(t)\hat{\boldsymbol{u}}_{ds,k} \qquad t = t_k \tag{53}$$

$$\hat{\boldsymbol{y}}_{ds,k} = \hat{\boldsymbol{C}}_{ds}(t)\hat{\boldsymbol{x}}_k^- + \hat{\boldsymbol{D}}_{ds}(t)\hat{\boldsymbol{u}}_{ds,k} \qquad t = t_k \tag{54}$$

where $\hat{\boldsymbol{x}}$ denotes the (virtual) state of the controller; $(\hat{\boldsymbol{u}}_{ct}, \hat{\boldsymbol{u}}_{ds,k})$ is the input of the controller, which equates to the output of the plant [i.e. $(\hat{\boldsymbol{u}}_{ct}, \hat{\boldsymbol{u}}_{ds,k}) = (\boldsymbol{y}_{ct}, \boldsymbol{y}_{ds,k})$]; $(\hat{\boldsymbol{y}}_{ct}, \hat{\boldsymbol{y}}_{ds,k})$ specifies the hybrid output of the controller, which is equal to the plant's input with negative sign under the assumption of sufficiently small disturbances $(\boldsymbol{d}_{ct}, \boldsymbol{d}_{ds}) \cong (\boldsymbol{0}, \boldsymbol{0})$ [i.e. $(\boldsymbol{u}_{ct}, \boldsymbol{u}_{ds,k}) = -(\hat{\boldsymbol{y}}_{ct}, \hat{\boldsymbol{y}}_{ds,k})$ as shown in Fig. 1]; and $\hat{\boldsymbol{x}}_k^{\pm} \triangleq \hat{\boldsymbol{x}}(t_k^{\pm})$ represent the controller's state vector immediately before and after impulsive actions at $t = t_k$. Furthermore, $\hat{\boldsymbol{A}}_{ct}$, $\hat{\boldsymbol{B}}_{ct}$, $\hat{\boldsymbol{C}}_{ct}$, $\hat{\boldsymbol{D}}_{ct}$, $\hat{\boldsymbol{A}}_{ds}$, $\hat{\boldsymbol{B}}_{ds}$, $\hat{\boldsymbol{C}}_{ds}$, and $\hat{\boldsymbol{D}}_{ds}$ denote the time-dependent system matrices, with appropriate dimensions, associated with the continuous-time and discrete-time subsystems of the compensator. The continuous evolutions and discontinuous changes occurring in the state of the controller due to the initial conditions $\hat{\boldsymbol{x}}_0$ and the input signals $(\hat{\boldsymbol{u}}_{ct}, \hat{\boldsymbol{u}}_{ds,k}) = (\boldsymbol{y}_{ct}, \boldsymbol{y}_{ds,k})$ can therefore be captured by:

$$\begin{cases} \dot{\hat{\boldsymbol{x}}}(t) = \hat{\boldsymbol{A}}_{ct}(t)\hat{\boldsymbol{x}} + \hat{\boldsymbol{B}}_{ct}(t)\boldsymbol{y}_{ct}(\boldsymbol{x}, t)\ ,\ \hat{\boldsymbol{x}}(\boldsymbol{0}) = \hat{\boldsymbol{x}}_0 & t \neq t_k \\ \hat{\boldsymbol{x}}_k^+ = \hat{\boldsymbol{A}}_{ds}(t)\hat{\boldsymbol{x}}_k^- + \hat{\boldsymbol{B}}_{ds}(t)\boldsymbol{y}_{ds,k} & t = t_k \end{cases} \tag{55}$$

Furthermore, with the continuous-time and discrete-time equations of output for $\mathcal{H}$ given by Eqs. (52) and (54) in mind and due to the fact that $(\hat{\boldsymbol{y}}_{ct}, \hat{\boldsymbol{y}}_{ds,k}) = -(\boldsymbol{u}_{ct}, \boldsymbol{u}_{ds,k})$, the hybrid control input to be fed back to the plant can then be formulated in the following interacting form:

$$\begin{cases} \boldsymbol{u}_{ct} = -\hat{\boldsymbol{C}}_{ct}(t)\hat{\boldsymbol{x}} - \hat{\boldsymbol{D}}_{ct}(t)\boldsymbol{y}_{ct} & t \neq t_k \\ \boldsymbol{u}_{ds,k} = -\hat{\boldsymbol{C}}_{ds}(t)\hat{\boldsymbol{x}}_k^- - \hat{\boldsymbol{D}}_{ds}(t)\boldsymbol{y}_{ds,k} & t = t_k \end{cases} \tag{56}$$

With the hybrid output of the plant satisfying the passivity specifications thus computed [$(\boldsymbol{y}_{ct}, \boldsymbol{y}_{ds,k})$ given by Eq. (47)], the main challenge is now to determine the time-dependent matrices involved in Eqs. (51)-(54) such that the input strict passivity requirements are met for $\mathcal{H}$. With this aim in view, the strict passivity-related KYP conditions represented by Eqs. (27)-(32) [corresponding to the structure of Eqs. (51)-(54) which are linear in $\hat{\boldsymbol{x}}$] are fed with $\mathcal{H}$-related system matrices and therefore employed. Considering $\mathcal{L}_{ct}$, $\mathcal{W}_{ct}$, γ_{ct}, $\mathcal{L}_{ds}$, $\mathcal{W}_{ds}$, and γ_{ds} as design

parameters to be appropriately chosen by the user, the proposed design procedure to rise to this challenge consists of three steps: in the first step, $\widehat{\boldsymbol{C}}_{ct}$, $\widehat{\boldsymbol{C}}_{ds}$, $\widehat{\boldsymbol{A}}_{ct}$, and $\widehat{\boldsymbol{A}}_{ds}$ are selected in a judicious manner to render the (underdetermined) equations (27)-(32) determined while simultaneously placing the poles of $\mathcal{H}$ at desired locations; the resulting differential and difference KYP equations [Eqs. (27) and (30) respectively] are then solved for $\mathcal{P}(t)$ in an interacting manner; and $\widehat{\boldsymbol{B}}_{ct}$, $\widehat{\boldsymbol{D}}_{ct}$, $\widehat{\boldsymbol{B}}_{ds}$, and $\widehat{\boldsymbol{D}}_{ds}$ are finally computed through the remaining KYP equations.

Instead of arbitrarily assigning $\widehat{\boldsymbol{C}}_{ct}$, $\widehat{\boldsymbol{C}}_{ds}$, $\widehat{\boldsymbol{A}}_{ct}$, and $\widehat{\boldsymbol{A}}_{ds}$, this paper proposes the hybrid linear quadratic regulator (LQR) policy [32], amongst all possible approaches, to accomplish the first objective. In this regard, a hybrid LQR formulation with finite-time horizon, which simultaneously combines the differential continuous-time Riccati equations with discrete-time Riccati events, is first set up as per the linearized equations of the plant to be controlled [Eqs. (17)-(20) where both continuous-time and discrete-time subsystems are assumed to be completely controllable and completely observable] in an attempt to render $\mathcal{H}$ asymptotically stable. Once the time-varying Riccati solutions are computed, the resultant continuous-time and discrete-time optimal gain matrices are then assigned to $\widehat{\boldsymbol{C}}_{ct}$ and $\widehat{\boldsymbol{C}}_{ds}$ respectively. Given a hybrid performance index of the form

$$\mathcal{J}=\int_{t_0}^{t_\mathrm{f}}\left(\boldsymbol{x}^{\mathrm{T}}(t)\boldsymbol{Q}_{ct}\boldsymbol{x}(t)+\boldsymbol{u}_{ct}^{\mathrm{T}}(\boldsymbol{x},t)\boldsymbol{R}_{ct}\boldsymbol{u}_{ct}(\boldsymbol{x},t)\right)dt+\sum_{k=1}^{\mathcal{K}}(\boldsymbol{x}_k^{-\mathrm{T}}\boldsymbol{Q}_{ds}\boldsymbol{x}_k^{-}+\boldsymbol{u}_{ds,k}^{\mathrm{T}}\boldsymbol{R}_{ds}\boldsymbol{u}_{ds,k}) \tag{57}$$

where $\mathcal{K}$ specifies the number of impulses applied during the operating time, and $\boldsymbol{Q}_{ct}=\boldsymbol{Q}_{ct}^{\mathrm{T}}\geq\boldsymbol{0}$, $\boldsymbol{R}_{ct}=\boldsymbol{R}_{ct}^{\mathrm{T}}>\boldsymbol{0}$, $\boldsymbol{Q}_{ds}=\boldsymbol{Q}_{ds}^{\mathrm{T}}\geq\boldsymbol{0}$, and $\boldsymbol{R}_{ds}=\boldsymbol{R}_{ds}^{\mathrm{T}}>\boldsymbol{0}$ denote the continuous-time and discrete-time weighting matrices acting on the state and control, it is well-known that the hybrid Riccati-based control law, which minimizes the hybrid performance index given by Eq. (57), can be obtained by the following pair of optimal control inputs [32]:

$$\begin{cases}\boldsymbol{v}_{ct}^{*} &= -\boldsymbol{R}_{ct}^{-1}\boldsymbol{B}_{ct}^{\mathrm{T}}\boldsymbol{\Gamma}(t)\boldsymbol{x}(t) & t\neq t_k\\ \boldsymbol{v}_{ds,k}^{*} &= -\boldsymbol{R}_{ds}^{-1}\boldsymbol{B}_{ds}^{\mathrm{T}}\boldsymbol{A}_{ds}^{-\mathrm{T}}\left[\boldsymbol{\Gamma}_k^{-}-\boldsymbol{Q}_{ds}\right]\boldsymbol{x}_k^{-} & t=t_k\end{cases} \tag{58}$$

wherein $\boldsymbol{\Gamma}(t)=\boldsymbol{\Gamma}^{\mathrm{T}}(t)\geq\boldsymbol{0}$ represent the time-varying Riccati solutions. In this regard, $\boldsymbol{\Gamma}(t)$ can be computed via integrating the following continuous-time set of differential Riccati equations backward in time from $t=t_\mathrm{f}$ to $t=0$ (given the terminal conditions $\boldsymbol{\Gamma}(t_\mathrm{f})=\boldsymbol{0}$) under the influence of jumps inducing in the matrix solution via provoking the discrete-time set of Riccati equations at $t=t_k$:

$$\begin{cases} \dot{\boldsymbol{\Gamma}}(t) + \boldsymbol{A}_{ct}^{\mathrm{T}}\boldsymbol{\Gamma}(t) + \boldsymbol{\Gamma}(t)\boldsymbol{A}_{ct} + \boldsymbol{Q}_{ct} - \boldsymbol{\Gamma}(t)\boldsymbol{B}_{ct}\boldsymbol{R}_{ct}^{-1}\boldsymbol{B}_{ct}^{\mathrm{T}}\boldsymbol{\Gamma}(t) = \boldsymbol{0}\ ,\ \boldsymbol{\Gamma}(t_{\mathrm{f}}) = \boldsymbol{0} & t \neq t_k \\ \boldsymbol{\Gamma}_k^{-} = \boldsymbol{Q}_{ds} + \boldsymbol{\Gamma}_k^{+} - \boldsymbol{\Gamma}_k^{+}\boldsymbol{B}_{ds}\left[\boldsymbol{R}_{ds} + \boldsymbol{B}_{ds}^{\mathrm{T}}\boldsymbol{\Gamma}_k^{+}\boldsymbol{B}_{ds}\right]^{-1}\boldsymbol{B}_{ds}^{\mathrm{T}}\boldsymbol{\Gamma}_k^{+} & t = t_k \end{cases} \tag{59}$$

With Eqs. (56) and (58) in mind, $\widehat{\boldsymbol{C}}_{ct}$ and $\widehat{\boldsymbol{C}}_{ds}$ are therefore determined as follows:

$$\widehat{\boldsymbol{C}}_{ct}(t) = \boldsymbol{R}_{ct}^{-1}\boldsymbol{B}_{ct}^{\mathrm{T}}\boldsymbol{\Gamma}(t) \tag{60}$$

$$\widehat{\boldsymbol{C}}_{ds}(t_k) = \boldsymbol{R}_{ds}^{-1}\boldsymbol{B}_{ds}^{\mathrm{T}}\boldsymbol{A}_{ds}^{-\mathrm{T}}\left[\boldsymbol{\Gamma}_k^{-} - \boldsymbol{Q}_{ds}\right] \tag{61}$$

Following the aforementioned hybrid LQR formulation, $\widehat{\boldsymbol{A}}_{ct}$ and $\widehat{\boldsymbol{A}}_{ds}$ are then selected such that the hybrid dynamic compensator represented by Eqs. (51)-(54) is asymptotically stable, that is:

$$\widehat{\boldsymbol{A}}_{ct}(t) = \boldsymbol{A}_{ct} - \boldsymbol{B}_{ct}\widehat{\boldsymbol{C}}_{ct} = \boldsymbol{A}_{ct} - \boldsymbol{B}_{ct}\boldsymbol{R}_{ct}^{-1}\boldsymbol{B}_{ct}^{\mathrm{T}}\boldsymbol{\Gamma}(t) \tag{62}$$

$$\widehat{\boldsymbol{A}}_{ds}(t_k) = \boldsymbol{A}_{ds} - \boldsymbol{B}_{ds}\widehat{\boldsymbol{C}}_{ds} = \boldsymbol{A}_{ds} - \boldsymbol{B}_{ds}\boldsymbol{R}_{ds}^{-1}\boldsymbol{B}_{ds}^{\mathrm{T}}\boldsymbol{A}_{ds}^{-\mathrm{T}}\left[\boldsymbol{\Gamma}_k^{-} - \boldsymbol{Q}_{ds}\right] \tag{63}$$

With $\widehat{\boldsymbol{A}}_{ct}$ and $\widehat{\boldsymbol{A}}_{ds}$ thus computed, the linear strict passivity-based gain matrix, $\mathcal{P}(t)$, can now be computed at each time instant through solving Eqs. (27) and (30) simultaneously as follows:

$$\begin{cases} \dot{\mathcal{P}}(t) + \widehat{\boldsymbol{A}}_{ct}^{\mathrm{T}}\mathcal{P}(t) + \mathcal{P}(t)\widehat{\boldsymbol{A}}_{ct} + \mathcal{L}_{ct}^{\mathrm{T}}\mathcal{L}_{ct} = \boldsymbol{0}\ ,\ \mathcal{P}(t_{\mathrm{f}}) = \mathcal{P}_{\mathrm{f}} & t \neq t_k \\ \mathcal{P}_k^{-} = \widehat{\boldsymbol{A}}_{ds}^{\mathrm{T}}\mathcal{P}_k^{+}\widehat{\boldsymbol{A}}_{ds} + \mathcal{L}_{ds}^{\mathrm{T}}\mathcal{L}_{ds} & t = t_k \end{cases} \tag{64}$$

where $\mathcal{P}_k^{\pm} \triangleq \mathcal{P}(t_k^{\pm})$, and $\mathcal{P}_{\mathrm{f}} = \mathcal{P}_{\mathrm{f}}^{\mathrm{T}} \geq \boldsymbol{0}$ specify the boundary conditions at the terminal time defined by the user as a design parameter. Analogous to the procedure explained in Sec. III.C, the continuous-time set of equations are first integrated backward in time to compute $\mathcal{P}(t)$ between impulsive instants, starting from the boundary conditions at the terminal time $\mathcal{P}_{\mathrm{f}}$. At each jump instant $t = t_k$, an instantaneous change is then induced in the matrix solution by arousing the discrete-time set of equations, and $\mathcal{P}_k^{-}$ computed at each jump is subsequently used as a new set of terminal conditions for the continuous-time set of equations to be integrated backward from t_k^{-} to t_{k-1}^{+}. This interacting procedure for calculating $\mathcal{P}(t)$ is continued until time zero is reached.

In the final step, simplifying assumptions in the form of $\mathcal{W}_{ct} \equiv \boldsymbol{0}$, $\boldsymbol{D}_{ct} = \boldsymbol{D}_{ct}^{\mathrm{T}}$, $\mathcal{W}_{ds} \equiv \boldsymbol{0}$, and $\boldsymbol{D}_{ds} = \boldsymbol{D}_{ds}^{\mathrm{T}}$ associated with the continuous-time and discrete-time subsystems are made to limit the design space, and $\widehat{\boldsymbol{B}}_{ct}$, $\widehat{\boldsymbol{D}}_{ct}$, $\widehat{\boldsymbol{B}}_{ds}$, and $\widehat{\boldsymbol{D}}_{ds}$ are ultimately computed through equations (28), (29), (31), and (32) respectively as follows:

$$\widehat{\boldsymbol{B}}_{ct}(t) = \boldsymbol{\mathcal{P}}^{-1}(t)\widehat{\boldsymbol{C}}_{ct}^{\mathrm{T}} \tag{65}$$

$$\widehat{\boldsymbol{D}}_{ct}(t) = \widehat{\boldsymbol{D}}_{ct} = \gamma_{ct}\mathbf{1}_{m_{ct}\times m_{ct}} \tag{66}$$

$$\widehat{\boldsymbol{B}}_{ds}(t_k) = \left(\widehat{\boldsymbol{A}}_{ds}^{\mathrm{T}}\boldsymbol{\mathcal{P}}_k^{+}\right)^{-1}\widehat{\boldsymbol{C}}_{ds}^{\mathrm{T}} \tag{67}$$

$$\widehat{\boldsymbol{D}}_{ds}(t_k) = \gamma_{ds}\mathbf{1}_{m_{ds}\times m_{ds}} + (1/2)\,\widehat{\boldsymbol{B}}_{ds}^{\mathrm{T}}\boldsymbol{\mathcal{P}}_k^{+}\widehat{\boldsymbol{B}}_{ds} \tag{68}$$

All the required ingredients are now in place to find the desired hybrid nonlinear passivity-based control law, the feedback of which to the plant endowed with passivity properties gives rise to the input-output stability of the closed-loop system. To this end, the hybrid output of the plant [$(\boldsymbol{y}_{ct}, \boldsymbol{y}_{ds,k})$ given by Eq. (47)] along with $\widehat{\boldsymbol{C}}_{ct}(t)$, $\widehat{\boldsymbol{C}}_{ds}$, $\widehat{\boldsymbol{D}}_{ct}(t)$, and $\widehat{\boldsymbol{D}}_{ds}$ [computed by Eqs. (60), (61), (66), and (68) respectively] are substituted into Eq. (56) so as to obtain the following interacting pair of passivity-based control inputs:

$$\begin{cases} \boldsymbol{u}_{ct}(\boldsymbol{x}, \hat{\boldsymbol{x}}, t) = -\boldsymbol{R}_{ct}^{-1}\boldsymbol{B}_{ct}^{\mathrm{T}}\boldsymbol{\Gamma}(t)\hat{\boldsymbol{x}}(t) - \dfrac{1}{2}\gamma_{ct}\boldsymbol{g}_{ct}^{\mathrm{T}}\mathbf{J}_x^{\mathrm{T}}\left(\boldsymbol{\Phi}_N(\boldsymbol{x})\right)\boldsymbol{\mathcal{C}}_N(t) & t \neq t_k \\ \boldsymbol{u}_{ds,k}(\boldsymbol{x}_k^-, \hat{\boldsymbol{x}}_k^-, t_k^+) = -\left(\mathbf{1}_{m_{ds}\times m_{ds}} + \widehat{\boldsymbol{D}}_{ds}\boldsymbol{j}_{ds}\right)^{-1}\left(\widehat{\boldsymbol{C}}_{ds}\hat{\boldsymbol{x}}_k^- + \widehat{\boldsymbol{D}}_{ds}\boldsymbol{h}_{ds}\right) & t = t_k \end{cases} \tag{69}$$

Therefore, the input-output stability of the closed-loop system is now guaranteed according to the passivity theorem via the negative feedback interconnection of the plant, which is passive, and the controller in the form of a dynamic compensator, which is input strictly passive.

IV. Spacecraft Attitude Kinematics and Dynamics

As a hybrid dynamical system, the attitude control system being proposed in this paper possesses two modes of operation: magnetic torquing, as a continuous-time renewable source of actuation, and impulsive thrusting exerted by expulsion devices (thrusters). The main motivation behind the collaborative utilization of magnetic and impulsive actuation, as stressed earlier, is to resolve instantaneous underactuation and gain limitations as the main drawbacks inherently associated with the magnetic attitude controllers, thereby improving system performance in terms of the accuracy of pointing and the speed of response. In this regard, the spacecraft operating in a low-Earth orbit is externally torqued by three mutually perpendicular magnetic torquers immersed in the Earth's magnetic field. Once a certain criterion is met, magnetic actuation is instantaneously switched to impulsive thrusting and, in turn, a triple set of impulsive torques, one about each direction of the body-fixed frame, is applied to the spacecraft. The attitude motion of the spacecraft is therefore characterized by a differential set of equations, which characterizes the

rotational motion of the dynamical system between impulsive events, and a set of difference equations, which governs instantaneous changes in the states of the system once an impulse occurs. Due to the cascade nature of the spacecraft attitude motion, the kinematic equations of motion must be coupled with the rotational dynamics. In this paper, the singularity-free four-parameter set of quaternions, $\boldsymbol{\varepsilon} = \begin{bmatrix} \varepsilon_1 & \varepsilon_2 & \varepsilon_3 \end{bmatrix}^{\mathrm{T}}$ and η, subject to the unit magnitude constraint, $\boldsymbol{\varepsilon}^{\mathrm{T}}\boldsymbol{\varepsilon} + \eta^2 = 1$, are elected to parameterize the attitude motion of the spacecraft. The kinematic equations of motion are therefore formulated as (Ref. [33] Chap. 2):

$$\begin{cases} \dot{\boldsymbol{\varepsilon}}(t) = (1/2)(\eta \mathbf{1}_{3\times 3} + \boldsymbol{\varepsilon}^{\times})\boldsymbol{\omega} \\ \dot{\eta}(t) = -(1/2)\boldsymbol{\varepsilon}^{\mathrm{T}}\boldsymbol{\omega} \end{cases} \tag{70}$$

where $\boldsymbol{\omega} = \begin{bmatrix} \omega_1 & \omega_2 & \omega_3 \end{bmatrix}^{\mathrm{T}}$ denotes the angular velocity vector and $(\cdot)^{\times}$ represents the skew-symmetric matrix used to implement the cross product. Armed with the spacecraft attitude kinematics, the rotational dynamics of the system are then described by Euler's rigid-body equations influenced by magnetic torques, $\boldsymbol{\tau}_{mag}$, impulsive thrusts applied at $t = t_k$, $\boldsymbol{\tau}_{imp}$, and external disturbance torques, $\boldsymbol{\tau}_{dis}$, as follows (Ref. [33] Chap. 4):

$$\boldsymbol{I}\dot{\boldsymbol{\omega}}(t) + \boldsymbol{\omega}^{\times}\boldsymbol{I}\boldsymbol{\omega} = \boldsymbol{\tau}_{mag} + \boldsymbol{\tau}_{imp} + \boldsymbol{\tau}_{dis} \tag{71}$$

where $\boldsymbol{I}$ is the spacecraft moment of inertia matrix. In addition, $\boldsymbol{\tau}_{mag}$ and $\boldsymbol{\tau}_{imp}$ can be obtained by (Ref. [33] Chap. 9):

$$\boldsymbol{\tau}_{mag} = \boldsymbol{m}^{\times}\boldsymbol{b}_{bf} \tag{72}$$

$$\boldsymbol{\tau}_{imp} = \sum_{k=1}^{\mathcal{K}} \boldsymbol{\nu}_k \delta(t - t_k) \tag{73}$$

wherein $\boldsymbol{m}$ is the commanded magnetic dipole moments generated by the magnetic torquers [i.e. $\boldsymbol{u}_{ct} = \boldsymbol{m}$], $\boldsymbol{b}_{bf}$ specifies the local geomagnetic field expressed in the body-fixed coordinate system, $\boldsymbol{\nu}_k$ denotes impulsive torque values produced by thrusters, and $\delta(t)$ is the Dirac delta function located at each impulsive instant t_k, the conjunction of which with $\boldsymbol{\nu}_k$ represents the discrete-time torque exerted on the spacecraft. Assuming the gravity-gradient disturbances and residual magnetic dipole moments resulting from onboard electronics as the most significant sources of disturbance for near-Earth small spacecraft, external disturbance torques can be found as ([33] Chap. 9):

$$\boldsymbol{\tau}_{dis} = \frac{3\mu}{\left\| \boldsymbol{r}_{bf} \right\|^5} \boldsymbol{r}_{bf}^{\times} \boldsymbol{I} \boldsymbol{r}_{bf} + \boldsymbol{m}_{dis}^{\times} \boldsymbol{b}_{bf} \tag{74}$$

where $\mu = 3.986 \times 10^{14}\ \mathrm{m}^3/\mathrm{sec}^2$ is the Earth's standard gravitational parameter, $\boldsymbol{r}_{bf}$ specifies the spacecraft position vector in the body-fixed frame, and $\boldsymbol{m}_{dis}$ denotes the residual magnetic dipole moments. Furthermore, a tilted dipole model of the geomagnetic field (as described in appendix H of Ref. [13]) is used in this paper to estimate the inertial magnetic field vector, $\boldsymbol{b}_{in}$. The rotation matrix from the Earth-Centered-Inertial (ECI) system to the body-fixed frame in terms of quaternions, $\mathcal{Q}_{bf-in}$, is ultimately employed to obtain $\boldsymbol{r}_{bf}$ and $\boldsymbol{b}_{bf}$ used in Eqs. (72) and (74) as below:

$$\mathcal{Q}_{bf-in}(\boldsymbol{\varepsilon}, \eta) = (1 - 2\boldsymbol{\varepsilon}^{\mathrm{T}}\boldsymbol{\varepsilon})\mathbf{1}_{3\times 3} + 2\boldsymbol{\varepsilon}\boldsymbol{\varepsilon}^{\mathrm{T}} - 2\eta\boldsymbol{\varepsilon}^{\times} \tag{75}$$

The spacecraft attitude control system, which collaboratively utilizes magnetic torques and impulsive thrusts to stabilize the spacecraft orientation, can therefore be formulated as the following hybrid nonlinear time-varying dynamical system:

$$\begin{cases} \begin{cases} \dot{\boldsymbol{\varepsilon}}(t) = (1/2)(\eta \mathbf{1}_{3\times 3} + \boldsymbol{\varepsilon}^{\times})\boldsymbol{\omega} \\ \dot{\eta}(t) = -(1/2)\boldsymbol{\varepsilon}^{\mathrm{T}}\boldsymbol{\omega} \\ \dot{\boldsymbol{\omega}}(t) = \boldsymbol{I}^{-1}(-\boldsymbol{\omega}^{\times}\boldsymbol{I}\boldsymbol{\omega} + \boldsymbol{\tau}_{mag} + \boldsymbol{\tau}_{dis}) \end{cases} & t \neq t_k \\ \Delta\boldsymbol{\omega}(t_k) = \boldsymbol{I}^{-1}\boldsymbol{\tau}_{imp} & t = t_k \end{cases} \tag{76}$$

V. Practical Considerations

This section serves to describe key factors in appropriately implementing the passivity-based control design frameworks developed in Sec. III. In what is to follow, the structure of the nonlinear time-varying dynamical system characterizing the attitude motion of the spacecraft with a hybrid source of actuation is first reviewed. The structural parameters, the judicious selection of which is required to accurately approximate the storage function involved in the differential and difference passivity-related KYP conditions [Eqs. (11) and (14) respectively] are then discussed in detail. The section ultimately proceeds with describing the major design parameters, the appropriate tuning of which significantly contribute to the satisfactory performance of the controllers being proposed.

By defining $\boldsymbol{x} = \left[\varepsilon_1 \quad \varepsilon_2 \quad \varepsilon_3 \quad \eta \quad \omega_1 \quad \omega_2 \quad \omega_3\right]^{\mathrm{T}}$, the continuous-time and discrete-time system functions involved in the attitude control system are therefore obtained by comparing Eqs. (1) and (3) to Eq. (76) as follows:

$$\boldsymbol{f}_{ct}(\boldsymbol{x},t)=\boldsymbol{f}_{ct}(\boldsymbol{x})=\begin{bmatrix}(1/2)(\eta\mathbf{1}_{3\times3}+\boldsymbol{\varepsilon}^{\times})\boldsymbol{\omega}\\-(1/2)\boldsymbol{\varepsilon}^{\mathrm{T}}\boldsymbol{\omega}\\-\boldsymbol{I}^{-1}\boldsymbol{\omega}^{\times}\boldsymbol{I}\boldsymbol{\omega}\end{bmatrix}\quad,\quad \boldsymbol{g}_{ct}(\boldsymbol{x},t)=\boldsymbol{g}_{ct}(\boldsymbol{\varepsilon},\eta,t)=\begin{bmatrix}\mathbf{0}_{4\times3}\\-\boldsymbol{I}^{-1}\boldsymbol{b}_{bf}^{\times}\end{bmatrix} \tag{77}$$

$$\boldsymbol{f}_{ds}(\boldsymbol{x}_k^-,t)=\boldsymbol{f}_{ds}(\boldsymbol{x}_k^-)=\boldsymbol{x}_k^-\quad,\quad \boldsymbol{g}_{ds}(\boldsymbol{x}_k^-,t)=\boldsymbol{g}_{ds}=\begin{bmatrix}\mathbf{0}_{4\times3}\\\boldsymbol{I}^{-1}\end{bmatrix} \tag{78}$$

Given the heterogeneous dynamics of the plant along with its interacting pair of outputs in nonlinear forms [Eqs. (1)-(4)], three major sets of parameters must appropriately be selected to approximate Eqs. (11) and (14) with sufficient accuracy as follows: a compact set that contains the origin as an interior point and is preferably symmetric about it, a set of basis functions that can adequately approximate the storage function involved in the passivity-related KYP conditions, and a set of collocation points that locates inside and on the boundaries of the compact set.

The compact set (or stability region or a bounded domain of the state space), $\boldsymbol{\Omega}$, is defined as the domain of possible values for the states. $\boldsymbol{\Omega}$ can be determined according to physical, kinematical, or practical limitations (physical capabilities) of the system, together with the likely deviation of the system states from their nominal value of zero. Due to the unit magnitude constraint acting on the quaternions, their domain of possible values is thus limited to $[-1\quad 1]$. Nevertheless, there are no kinematical limitations for angular velocity components and their stability region is accordingly chosen on the basis of practical considerations (as expressed in rad/s). The stability region for the problem in hand can therefore be defined as:

$$\boldsymbol{\Omega}=[-1\quad 1]_{\varepsilon_1}\times[-1\quad 1]_{\varepsilon_2}\times[-1\quad 1]_{\varepsilon_3}\times[-1\quad 1]_{\eta}\times[-1\quad 1]_{\omega_1}\times[-1\quad 1]_{\omega_2}\times[-1\quad 1]_{\omega_3}$$

Proper selection of basis functions is also critical to design the nonlinear passivity-based controllers in question. Two important requirements, namely *characteristic* and *quantity requirements*, pertaining to the structure and number of basis elements must be satisfied in order to make an appropriate choice of basis functions. The main objective being pursued by the characteristic requirement is to synthesize a controller by which the essential nonlinear terms involved in the dynamics are effectively captured. Basis elements are therefore configured such that the constituent linear and nonlinear terms of the system dynamics are incorporated into the control law. The controller is consequently endowed with authority to adequately compensate for the nonlinear dynamics of the system. Furthermore, the number of basis elements must be sufficiently large to approximate the storage function with sufficient accuracy (*quantity requirement*). The accuracy of V_N is therefore dependent on both characteristics and quantities of the basis elements elected to form the approximation.

As demonstrated in the literature, polynomials are proven to work effectively as basis functions in algorithms wherein the Galerkin-based projection is used to approximate partial derivative equations such as the Hamilton-Jacobi-Bellman [34, 35] and Hamilton-Jacobi-Isaac [36] equations. To the knowledge of the current authors, the best way to find an appropriate selection of basis functions for time-varying dynamical systems is to commence with the quadratic basis elements obtained by the second-order expansion of the states, eliminating those terms whose corresponding control gains are either zero or very small as compared to the other terms. The remaining quadratic basis elements must then be augmented by further higher-order terms to capture the dominant nonlinear dynamics of the system. Due to multiplication of $\boldsymbol{g}_{ct}^{\mathrm{T}}(\boldsymbol{x},t)$ and $\boldsymbol{g}_{ds}^{\mathrm{T}}(\boldsymbol{x}_k,t_k)$ with $\mathbf{J}_{\boldsymbol{x}}^{\mathrm{T}}\left(\boldsymbol{\Phi}_N(\boldsymbol{x})\right)$ in the passivity-based control laws given by Eqs. (50) and (69), these additional higher-order basis elements must be selected such that their partial derivatives with respect to *gain-effective states* (those states which correspond to non-zero elements of $\boldsymbol{g}_{ct}^{\mathrm{T}}(\boldsymbol{x},t)$ and $\boldsymbol{g}_{ds}^{\mathrm{T}}(\boldsymbol{x}_k,t_k)$ in Eqs. (50) and (69), thereby contributing substantially to preserve non-zero control gains) result in functions of the states desired to ultimately appear in the passivity-based control laws in order to capture the essential nonlinear dynamics of the system.

By considering the structure of $\boldsymbol{g}_{ct}(\boldsymbol{x},t)$ and $\boldsymbol{g}_{ds}(\boldsymbol{x}_k,t_k)$ for the hybrid attitude control system in question [as shown in (77) and (78) respectively], angular velocity components (ω_1, ω_2, and ω_3) act as the gain-effective states for this problem. Therefore, any basis element consisting of either ω_1, ω_2, or ω_3 (or their combinations) will ultimately show up in the passivity-based control laws as demonstrated below:

$$
\begin{aligned}
\boldsymbol{u}_{ct}(\boldsymbol{x},t) &= -\frac{1}{2}\boldsymbol{K}_{ct}\boldsymbol{g}_{ct}^{\mathrm{T}}\mathbf{J}_{\boldsymbol{x}}^{\mathrm{T}}\left(\boldsymbol{\Phi}_N(\boldsymbol{x})\right)\boldsymbol{C}_N(t) \\
&= -\frac{1}{2}\boldsymbol{K}_{ct}\begin{bmatrix} 0 & 0 & 0 & 0 & 0 & g_{61} & g_{71} \\ 0 & 0 & 0 & 0 & g_{52} & 0 & g_{72} \\ 0 & 0 & 0 & 0 & g_{53} & g_{63} & 0 \end{bmatrix}\begin{bmatrix} \dfrac{\partial\phi_1}{\partial\varepsilon_1} & \cdots & \dfrac{\partial\phi_N}{\partial\varepsilon_1} \\ \vdots & \ddots & \vdots \\ \dfrac{\partial\phi_1}{\partial\omega_3} & \cdots & \dfrac{\partial\phi_N}{\partial\omega_3} \end{bmatrix}\begin{bmatrix} c_1(t) \\ \vdots \\ c_N(t) \end{bmatrix} \\
&= -\frac{1}{2}\boldsymbol{K}_{ct}\begin{bmatrix} g_{61}\dfrac{\partial\phi_1}{\partial\omega_2}+g_{71}\dfrac{\partial\phi_1}{\partial\omega_3} & \cdots & g_{61}\dfrac{\partial\phi_N}{\partial\omega_2}+g_{71}\dfrac{\partial\phi_N}{\partial\omega_3} \\ g_{52}\dfrac{\partial\phi_1}{\partial\omega_1}+g_{72}\dfrac{\partial\phi_1}{\partial\omega_3} & \cdots & g_{52}\dfrac{\partial\phi_N}{\partial\omega_1}+g_{72}\dfrac{\partial\phi_N}{\partial\omega_3} \\ g_{53}\dfrac{\partial\phi_1}{\partial\omega_1}+g_{63}\dfrac{\partial\phi_1}{\partial\omega_2} & \cdots & g_{53}\dfrac{\partial\phi_N}{\partial\omega_1}+g_{63}\dfrac{\partial\phi_N}{\partial\omega_2} \end{bmatrix}\begin{bmatrix} c_1(t) \\ \vdots \\ c_N(t) \end{bmatrix}
\end{aligned}
$$

wherein g_{52}, g_{53}, g_{61}, g_{63}, g_{71}, and g_{72} represent non-zero elements of $\boldsymbol{g}_{ct}(\boldsymbol{x},t)$. Similar derivation can simply be obtained for the discrete-time passivity-based control law while the gain-effective states are identical. With an attitude controller composing of quaternion-based proportional control and $\boldsymbol{\omega}$-based rate control in mind, an initial set of quadratic basis elements, the partial derivatives of which with respect to the gain-effective states produce all the required components of $\boldsymbol{\varepsilon}$ (for proportional control) and $\boldsymbol{\omega}$ (for rate control) in the passivity-based control laws, are first chosen to construct the desired proportional-derivative (PD) control scheme, while simultaneously meeting the characteristic requirement as follows: $\left\{\varepsilon_1\omega_1, \omega_1^2, \varepsilon_2\omega_2, \omega_2^2, \varepsilon_3\omega_3, \omega_3^2\right\}$. This choice must, however, be complemented by $\left\{\varepsilon_1^2, \varepsilon_2^2, \varepsilon_3^2, (\eta-1)^2\right\}$ to satisfy the positive-definiteness properties of the storage function.

Basis functions satisfying the characteristic requirement are then augmented by some additional higher-order terms to guarantee the accuracy of the approximation. By gradual increase in the number of basis elements in a manner consistent with the characteristic requirement, V_N gradually approaches to V. At a certain number of basis elements, the satisfactory performance is ultimately obtained and, in consequence, the quantity requirement is fulfilled, i.e. $V_N \cong V$. Henceforth, any further increase in the number of basis elements yields insignificant improvement in the system performance at the expense of computational cost. This process requires a deep understanding of the dynamical behavior of the system being considered, as well as trial and error. In addition to characteristic and quantity requirements stressed in the preceding, an appropriate choice of basis functions must also produce an invertible $\left\langle \boldsymbol{\Phi}_N, \boldsymbol{\Phi}_N \right\rangle_{\boldsymbol{\Omega}}$ matrix to satisfy the rank condition required by Eq. (38). In view of the preceding guidelines, the following 28 basis elements are consequently selected as basis functions for this problem to discretize the storage function involved in the passivity-related KYP conditions:

$$\begin{aligned}\boldsymbol{\Phi}_N = \big\{&\varepsilon_1^2, \varepsilon_1\omega_1, \omega_1^2,\ \varepsilon_2^2, \varepsilon_2\omega_2, \omega_2^2,\ \varepsilon_3^2, \varepsilon_3\omega_3, \omega_3^2,\ (\eta-1)^2,\\ &\varepsilon_1^4, \varepsilon_1^2\omega_1^2, \omega_1^4,\ \varepsilon_2^4, \varepsilon_2^2\omega_2^2, \omega_2^4,\ \varepsilon_3^4, \varepsilon_3^2\omega_3^2, \omega_3^4,\\ &\varepsilon_1^4\omega_1^2, \varepsilon_2^4\omega_2^2, \varepsilon_3^4\omega_3^2,\ \varepsilon_1^7\omega_1, \varepsilon_2^7\omega_2, \varepsilon_3^7\omega_3,\ \varepsilon_1^5\omega_1^3, \varepsilon_2^5\omega_2^3, \varepsilon_3^5\omega_3^3\big\}\end{aligned}$$

A suitable set of collocation points $\bar{\boldsymbol{x}} = \underset{m}{\text{row}}\left\{\bar{\boldsymbol{x}}_m\right\}$, wherein $\bar{\boldsymbol{x}}_m \in \mathbb{R}^7$ and $m = 1,...,28$, is also necessary to design the discrete-time nonlinear passivity-based controller. Collocation points can be selected from the entire compact set excluding the origin, provided the rank condition required to produce an invertible $\boldsymbol{\Psi}_k(\bar{\boldsymbol{x}})$ in Eq. (41) is satisfied.

With the structural parameters $\boldsymbol{\Omega}$, $\boldsymbol{\Phi}_N$, and $\bar{\boldsymbol{x}}$ thus discussed, the boundary conditions at the terminal time, $\boldsymbol{\mathcal{C}}_{\text{f}}$, impulsive application times, $\left\{t_1,...,t_{\mathcal{K}}\right\}$, and weighting functions, $\boldsymbol{l}_{ct}$ and $\boldsymbol{l}_{ds}$, remain to be appropriately determined as

design parameters in order to compute the passivity-based control gains to be fed to the passivity-based control laws being proposed. Amongst all design parameters which acquire significance in satisfying the passivity specifications of the plant, the boundary conditions at the terminal time, $\mathcal{C}_{\mathrm{f}}$, play a crucial role. Owing to the time-varying nature of the passivity-based control gains $\mathcal{C}_N(t)$, blind selection of $\mathcal{C}_{\mathrm{f}}$ can lead undesirable gains with unbounded growth in $\mathcal{C}_N(t)$ backward, thereby destroying the control design. Every components of $\mathcal{C}_{\mathrm{f}}$ must thus receive careful attention in order to produce acceptable results. The boundary conditions at the terminal time for this problem are set to be:

$$\begin{aligned}\mathcal{C}_{\mathrm{f}} = \{ & c_\varepsilon, c_{\varepsilon\omega^1}, c_\omega \ , \ c_\varepsilon, c_{\varepsilon\omega^1}, c_\omega \ , \ c_\varepsilon, c_{\varepsilon\omega^1}, c_\omega \ , \ c_\eta, \\ & c_\varepsilon, c_{\varepsilon\omega}, c_\omega \ , \ c_\varepsilon, c_{\varepsilon\omega}, c_\omega \ , \ c_\varepsilon, c_{\varepsilon\omega}, c_\omega \ , \\ & c_{\varepsilon\omega}, c_{\varepsilon\omega}, c_{\varepsilon\omega} \ , \ c_{\varepsilon\omega^1}, c_{\varepsilon\omega^1}, c_{\varepsilon\omega^1} \ , \ c_{\varepsilon\omega}, c_{\varepsilon\omega}, c_{\varepsilon\omega} \}\end{aligned}$$

wherein $c_\varepsilon = 0$ and $c_\omega = 2\times10^9$, respectively, correspond to the basis elements involving even orders of ε_i and ω_i alone with $i = 1,...,3$; $c_\eta = 0$ is associated with $(\eta-1)^2$; $c_{\varepsilon\omega^1} = 4\times10^6$ is related to the basis elements consisting of cross-terms of ε_i and ω_i where ω_i is of first order (i.e. $\varepsilon_i\omega_i$ and $\varepsilon_i^7\omega_i$ which lead to sole components of ε_i in the passivity-based control laws); and $c_{\varepsilon\omega} = 8\times10^6$ matches the remaining basis elements involving cross-terms of ε_i and ω_i which create terms of $\varepsilon_i\omega_i$ in the control scheme being proposed.

Assuming a prescribed sequence of impulsive times, eight equally-spaced impulses are selected for this problem as represented in terms of true anomaly in the following: $\boldsymbol{\theta}_k = \{5^\circ, 50^\circ, 95^\circ, 140^\circ, 185^\circ, 230^\circ, 275^\circ, 320^\circ\}$. This choice, the selection of which is based upon various simulations, suggests the firing times through which satisfactory performance is obtained for the attitude control system in question.

Furthermore, in harmony with the linear design approach, $\boldsymbol{l}_{ct}$ and $\boldsymbol{l}_{ds}$ in this paper are selected to be in the form of $\boldsymbol{l}_{ct}(\boldsymbol{x},t) = \boldsymbol{L}_{ct}\boldsymbol{x}$ and $\boldsymbol{l}_{ds}(\boldsymbol{x}_k^-, t_k^-) = \boldsymbol{L}_{ds}\boldsymbol{x}_k^-$ [See Eqs. (38) and (42)], where $\boldsymbol{L}_{ct}$ and $\boldsymbol{L}_{ds}$ are assumed to be constant. As a direct consequence, $\boldsymbol{l}_{ct}^{\mathrm{T}}\boldsymbol{l}_{ct} = \boldsymbol{x}^{\mathrm{T}}\boldsymbol{\Theta}_{ct}\boldsymbol{x}$ and $\boldsymbol{l}_{ds}^{\mathrm{T}}\boldsymbol{l}_{ds} = \boldsymbol{x}_k^{-\mathrm{T}}\boldsymbol{\Theta}_{ds}\boldsymbol{x}_k^-$ wherein $\boldsymbol{\Theta}_{ct} = \boldsymbol{L}_{ct}^{\mathrm{T}}\boldsymbol{L}_{ct} \in \mathbb{R}^{n\times n}$ and $\boldsymbol{\Theta}_{ds} = \boldsymbol{L}_{ds}^{\mathrm{T}}\boldsymbol{L}_{ds} \in \mathbb{R}^{n\times n}$ represent symmetric positive semi-definite weighting matrices associated with the continuous-time and discrete-time subsystems respectively. The aforementioned matrices can therefore be taken outside the integrals, thereby tuning the system computationally fast. In this paper, the following matrices are selected to weight Eq. (46):

$$\boldsymbol{\Theta}_{ct} = diag(1 \quad 1 \quad 1 \quad 0 \quad 10^2 \quad 10^2 \quad 10^2) \quad , \quad \boldsymbol{\Theta}_{ds} = diag(1 \quad 1 \quad 1 \quad 0 \quad 10^2 \quad 10^2 \quad 10^2)$$

Lastly, all computations involved in the proposed hybrid control algorithms are performed off-line (prior to implementation); once the passivity-based control gains, $\mathcal{C}_N(t)$, are computed through numerically solving Eq. (46), the proposed control schemes can be implemented in hardware and run in real time. Moreover, there are some possibilities to facilitate the implementation process. For instance, assuming a periodic or quasi-periodic character for the passivity-based control gains over the operating time, Fourier series can be employed to approximate the steady-state part of $\mathcal{C}_N(t)$ by discarding the initial transient phase coming backward from t_f. Rather than storing the entire time history of $\mathcal{C}_N(t)$, the Fourier coefficients resulting from the Fourier-based approximation can be stored onboard. As a consequence, not only is the storage memory requirement significantly reduced, but also $\mathcal{C}_N(t)$ computed by a backward integration process prior to implementation is no longer restricted to the time interval from 0 to t_f (defined by the user during control design) and can, in turn, be extended to any desired operating time. Analogous comments are also held for $\Gamma(t)$ and $\mathcal{P}(t)$ (See Eqs. (59) and (64) respectively).

VI. Numerical Simulations

In this section, the passivity-based control design frameworks developed in Secs. III.D and III.E are exploited to synthesize controllers of a nonlinear nature for stabilizing the attitude motion of spacecraft with magnetic and impulsive sources of actuation. The control objective here is to regulate the vector part of quaternions and angular velocity components to zero, while simultaneously rejecting the external disturbance torques given by Eq. (74). Assuming a spacecraft with the moment of inertia matrix $\boldsymbol{I} = diag\begin{pmatrix}27 & 17 & 25\end{pmatrix}\ \mathrm{kg\cdot m^2}$ and the residual magnetic dipole moments $\boldsymbol{m}_{dist} = [0.1 \quad 0.1 \quad 0.1]^{\mathrm{T}}\ \mathrm{A\cdot m^2}$ travelling in a circular Keplerian orbit at an altitude of 450 km, the classical orbital elements used in this paper to describe the orbital motion of the spacecraft in the ECI coordinate system are defined as: $\left\{a, e, \hat{i}, \hat{\Omega}, \hat{\omega}, t_0\right\} = \left\{6820\,\mathrm{km}, 0, 87^{\circ}, 0, 0, 0\right\}$; where a, e, $\hat{i}$, $\hat{\Omega}$, $\hat{\omega}$, and t_0 denote the semi-major axis, eccentricity, inclination, right ascension of the ascending node, argument of perigee, and time of perigee passage respectively.

Aiming to compute the passivity-based control gains, the utilization of which in the hybrid output dynamics of the plant [given by Eq. (47)] satisfy the passivity specifications, the hybrid numerical algorithm derived in Sec. III.C is first erected via appropriate sets of structural and design parameters, as described in Sec. V. Interconnecting the resultant passive plant with input strictly passive compensators of static and dynamic forms through a negative

feedback, the hybrid control architectures developed in Secs. III.D and III.E are ultimately used in Secs. VI.A and VI.B respectively to regulate the attitude motion of the spacecraft in question.

In order to evaluate the efficacy of employing a hybrid control architecture (as against a single-mode magnetic one) and a nonlinear control design approach (as opposed to a linear one) in synthesizing the passivity-based controllers developed in Secs. III.D and III.E, two additional magnetic passivity-based attitude controllers are also designed and tested in this section by using the identical sets of design parameters and initial conditions: a single-mode magnetic (without impulsive thrusts) nonlinear passivity-based controller designed via considering the full nonlinear kinematics and dynamics of the system, which utilizes only the continuous-time portion of the proposed algorithms in Secs. III.D and III.E; and a hybrid (magnetic and impulsive) linear passivity-based controller founded upon the linearized rotational equations of motion with the following system matrices, which in fact employs the passivity-related KYP conditions given by Eqs. (21)-(26) to compute the interacting pair of outputs through which the passivity specifications for the linearized plant are fulfilled:

$$\boldsymbol{A}_{ct}(t)=\boldsymbol{A}_{ct}=\begin{bmatrix}\boldsymbol{0}_{3\times3} & (1/2)\boldsymbol{1}_{3\times3}\\ \boldsymbol{0}_{3\times3} & \boldsymbol{0}_{3\times3}\end{bmatrix}\quad,\quad \boldsymbol{B}_{ct}(t)=\begin{bmatrix}\boldsymbol{0}_{3\times3}\\ -\boldsymbol{I}^{-1}\boldsymbol{b}_{in}^{\times}\end{bmatrix} \tag{79}$$

$$\boldsymbol{A}_{ds}(t_k)=\boldsymbol{A}_{ds}=\boldsymbol{1}_{6\times6}\quad,\quad \boldsymbol{B}_{ds}(t_k)=\boldsymbol{B}_{ds}=\begin{bmatrix}\boldsymbol{0}_{3\times3}\\ \boldsymbol{I}^{-1}\end{bmatrix} \tag{80}$$

Furthermore, the following root-mean-square (RMS) norms are also defined and computed over 15 orbits to quantitatively assess the performance of the proposed hybrid nonlinear controllers as against the other two ones:

$$\begin{gathered}\overline{\|\phi\|}=\sqrt{\frac{\int_0^{15\mathcal{T}}\phi^2(t)dt}{15\mathcal{T}}}\ (\text{rad})\quad,\quad \overline{\|\boldsymbol{\omega}\|}=\sqrt{\frac{\int_0^{15\mathcal{T}}\boldsymbol{\omega}^{\mathrm{T}}(t)\boldsymbol{\omega}(t)dt}{15\mathcal{T}}}\ (\text{rad/s})\\ \overline{\|\boldsymbol{\tau}_{mag}\|}=\sqrt{\frac{\int_0^{15\mathcal{T}}\boldsymbol{\tau}_{mag}^{\mathrm{T}}(t)\boldsymbol{\tau}_{mag}(t)dt}{15\mathcal{T}}}\ (\text{N}\cdot\text{m})\quad,\quad \overline{\|\boldsymbol{\tau}_{imp}\|}=\sqrt{\frac{\sum_{k=1}^{\mathcal{K}}(\boldsymbol{u}_{ds,k}^{\mathrm{T}}\boldsymbol{u}_{ds,k})}{\mathcal{K}}}\ (\text{N}\cdot\text{m})\end{gathered} \tag{81}$$

where $\phi(t)=\cos^{-1}\left(\left(\text{trace}\left[\mathcal{Q}_{bf-in}\right]-1\right)/2\right)$ is the rotation angle (as expressed in rad) of the spacecraft from Euler axis-angle parameters and $\mathcal{T}$ denotes the orbital period. In this regard, the norms of rotation angle and impulsive torque, $\overline{\|\phi\|}$ and $\overline{\|\boldsymbol{\tau}_{imp}\|}$, can be used as important criteria for accurate pointing and efficient fuel missions respectively. By adjusting the size of the diagonal terms in the weighting matrices involved in the proposed control algorithms, a trade-off between accuracy and fuel expenditure can be made to achieve a high precision pointing with low fuel

requirements. Furthermore, the norm of magnetic torque, $\overline{\|\boldsymbol{\tau}_{mag}\|}$, can be employed to evaluate the feasibility of the attitude controller in terms of the magnetic control usage required by torque rods for stabilization purposes.

Lastly, the power required by actuation mechanisms during a mission can be used as a key factor to determine the feasibility of a control scheme proposed for regulating the attitude motion of a spacecraft. Assuming the spacecraft being considered is equipped with three magnetic torquers composed of loops of the cross-sectional area $\mathcal{A} = \pi d^2/4 \ \text{m}^2$, where $d = 10$ mm, with $\mathcal{N} = 400$ turns of wire and the electrical resistance of $\mathcal{R} = 100\ \Omega$, the electrical energy consumed by magnetic torquers during the operating time can be estimated and, therefore, used as the means by which the performance of all magnetic attitude controllers is assessed and compared as follows [13]:

$$\mathcal{E} = \frac{3\mathcal{R}}{\mathcal{N}^2\mathcal{A}^2}\int_{t_0}^{t_f} \boldsymbol{m}^{\mathrm{T}}\boldsymbol{m}\, dt \tag{82}$$

All the required ingredients are now in place to utilize the hybrid control architectures proposed in Secs. III.D and III.E for regulating the attitude motion of the spacecraft. This is the subject of the following two sections.

A. Attitude Regulation via Static Compensator

The passivity-based control design framework developed in Sec. III.D, which uses a constant-gain static compensator in its feedback loop to comply with the passivity theorem, is employed in this section to regulate the spacecraft attitude motion. To this end, the continuous-time and discrete-time positive proportional control gains used in the feedback loop to guarantee input strict passivity are tuned to $\boldsymbol{K}_{ct} = (9\times10^{-1})\mathbf{1}_{3\times3}$ and $\boldsymbol{K}_{ds} = (5\times10^{-7})\mathbf{1}_{3\times3}$ respectively. The numerical results obtained by simulating the behavior of the attitude control system equipped with the hybrid passivity-based constant-gain static compensator are depicted in Figs. 2 and 3 along with Table 1 under the influence of the initial conditions $\boldsymbol{\varepsilon}_0 = \begin{bmatrix}0.5 & 0.5 & 0.5\end{bmatrix}^{\mathrm{T}}$, $\eta_0 = 0.5$, and $\boldsymbol{\omega}_0 = \begin{bmatrix}0.1 & 0.1 & 0.1\end{bmatrix}^{\mathrm{T}}$ rad/s.

Shown in Figs. 2 and 3, the effectiveness of using a nonlinear control approach as compared to a linear one in the proposed hybrid passivity-based attitude control architecture is depicted in terms of system response and control usage. As is apparent from Fig. 2, the hybrid nonlinear attitude controller outperforms significantly the hybrid linear control scheme when transient response is concerned. Specifically, whereas the settling time for $\boldsymbol{\varepsilon}$ is approximately one orbit for the attitude control system equipped with hybrid nonlinear control scheme, these quantities are settled after six orbits for the system which uses a hybrid linear controller. Moreover, Fig. 3 demonstrates significant reduction in both magnetic and impulsive control torques via employing the hybrid nonlinear control approach in

comparison with the hybrid linear one which, in consequence, facilitates the feasibility of the attitude control system by eliminating excessive load on each actuator.

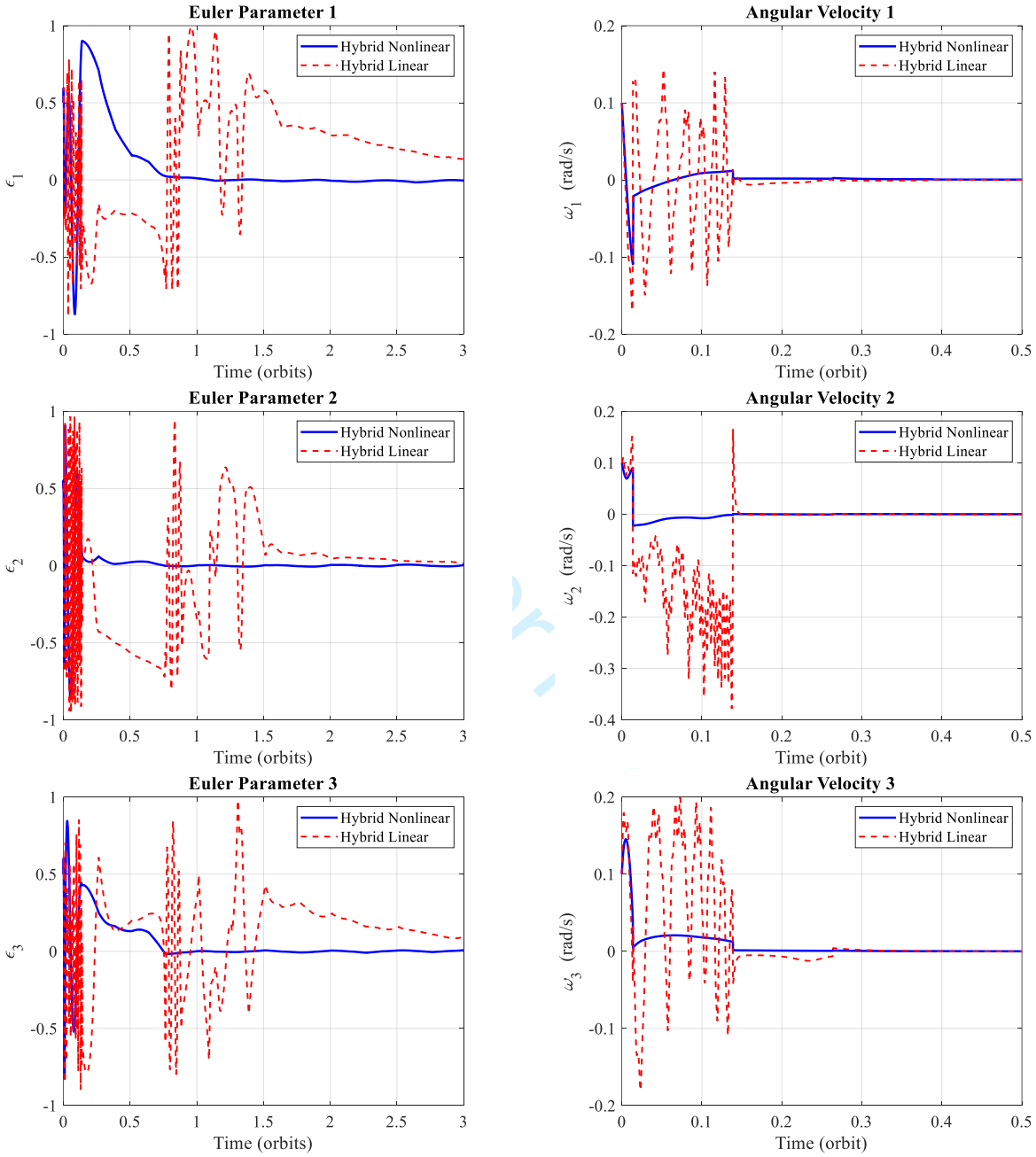

Fig. 2. Time histories of Euler parameters (left column) and angular velocity components (right column) for hybrid nonlinear and linear passivity-based attitude control schemes with static compensator

Table 1 also summarizes and compares the results obtained by quantitatively assessing the performance of all three passivity-based attitude controllers via Eqs. (81) and (82). As is obvious, noticeable improvement in all parameters associated with the hybrid nonlinear controller is evident as against the other two ones. For instance, $\overline{\|\phi\|}$

and $\overline{\|\boldsymbol{\tau}_{imp}\|}$, which represent a trade-off between accuracy and fuel expenditure as stressed earlier, experience 47.42 and 71.69 percent improvement respectively for the hybrid nonlinear controller beside the hybrid linear one.

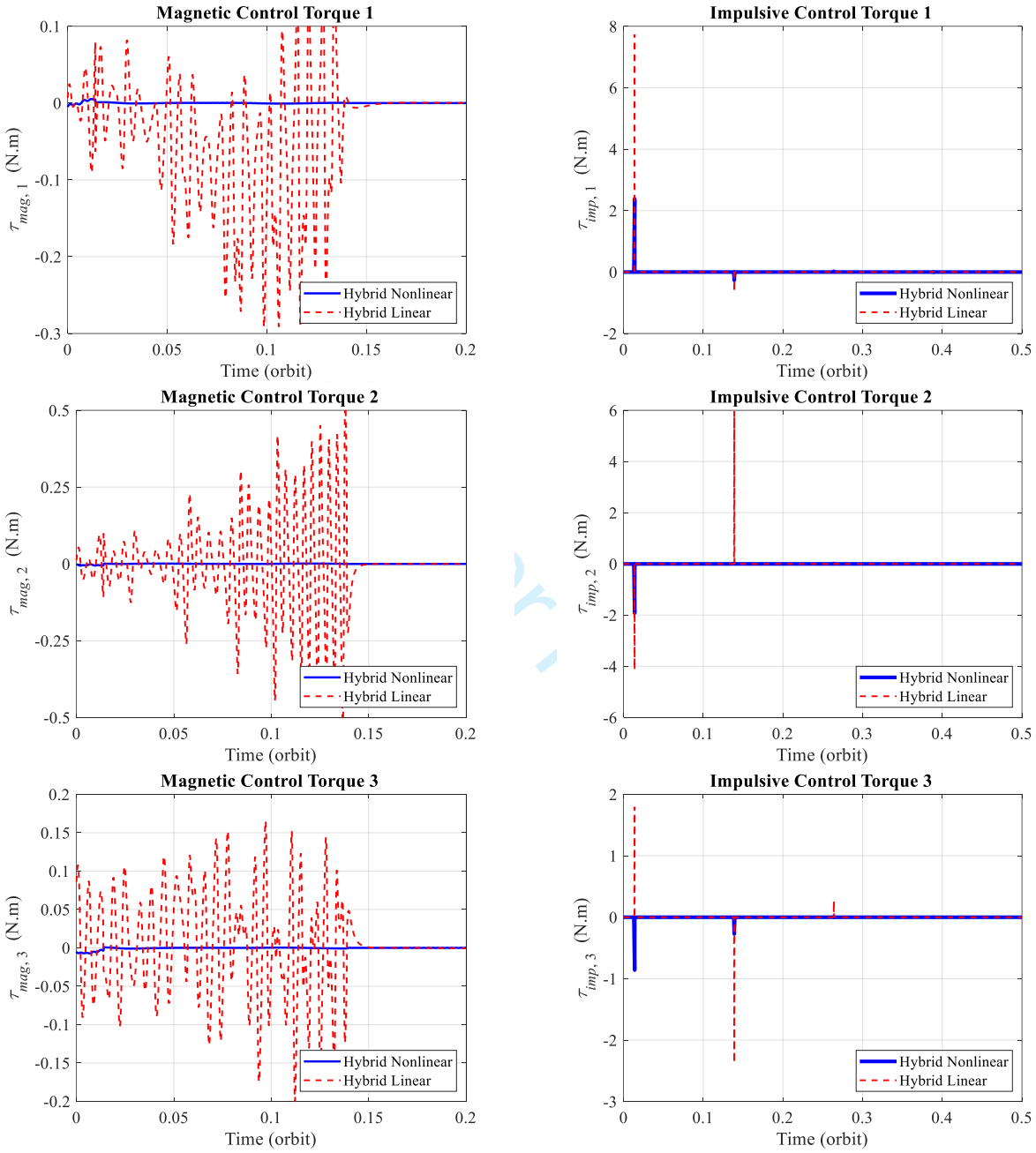

Fig. 3. Time histories of magnetic (left column) and impulsive (right column) control torques for hybrid nonlinear and linear passivity-based attitude control schemes with static compensator

Furthermore, whereas the required magnetic torque for stabilizing the spacecraft via the proposed hybrid nonlinear control scheme is $2.55\times10^{-4}\ \mathrm{N\cdot m}$, and consequently lies within the acceptable range of 10^{-5} to $10^{-3}\ \mathrm{N\cdot m}$ as demonstrated in Refs. [14, 15], magnetic torque of value $2.01\times10^{-2}\ \mathrm{N\cdot m}$ is necessary for the hybrid linear

controller to attain the identical objective. The maximum obtainable magnetic dipole moments of the magnetic torqrods associated with the hybrid linear system must accordingly be increased by significantly enlarging the torqrods, which is practically impossible.

Table 1. Functional performance of hybrid nonlinear attitude control scheme equipped with static compensator in comparison to hybrid linear and magnetic-only nonlinear control laws

	Parameter	$\mathcal{E}$	$\overline{\|\phi\|}$	$\overline{\|\omega\|}$	$\overline{\|\tau_{mag}\|}$	$\overline{\|\tau_{imp}\|}$
Control Policy	Hybrid Nonlinear Passive (**HNP**)	2.57×10^{12}	4.04×10^{-1}	5.26×10^{-3}	2.55×10^{-4}	2.88×10^{-1}
	Hybrid Linear Passive (**HLP**)	1.42×10^{16}	7.68×10^{-1}	2.13×10^{-2}	2.01×10^{-2}	1.02×10^{0}
	Magnetic Nonlinear Passive (**MNP**)	8.40×10^{12}	7.59×10^{-1}	1.07×10^{-2}	5.36×10^{-4}	-
Improvement	**HNP** as compared to **HLP**	99.98 %	47.42 %	75.31 %	98.73 %	71.69 %
	HNP as compared to **MNP**	69.39 %	46.85 %	50.77 %	52.39 %	-
	MNP as compared to **HLP**	99.94 %	1.10 %	49.85 %	97.34 %	-

B. Attitude Regulation via Dynamic Compensator

In the next attempt, the passivity-based control algorithm proposed in Sec. III.E, which employs a dynamic compensator in its feedback loop, is used to regulate the spacecraft attitude motion. To this end, the following weighting matrices are first elected for the proposed hybrid LQR architecture formulated by Eq. (59), the objective of which is to compute the time-varying Riccati gain matrix $\boldsymbol{\Gamma}(t)$ to be used in Eqs. (60) and (61), in preparation for placing the poles of the dynamic compensator in question at desired locations:

$$\boldsymbol{Q}_{ct} = (8\times10^{5})\mathbf{1}_{6\times6} \quad , \quad \boldsymbol{R}_{ct} = (10^{7})\mathbf{1}_{3\times3}$$

$$\boldsymbol{Q}_{ds} = (10^{10})\mathbf{1}_{6\times6} \quad , \quad \boldsymbol{R}_{ds} = (3\times10^{13})\mathbf{1}_{3\times3}$$

Next, the following parameters are chosen to simultaneously erect the interacting sets of equations given by (64) to be integrated backward in time from $t = t_{\mathrm{f}}$ to $t = 0$, while instantaneously switching to the discrete-time events at $t = t_k$ where $0 < t_k < t_{\mathrm{f}}$, in order to compute $\mathcal{P}(t)$ at each time instant to be used in Eqs. (65), (67), and (68):

$$\boldsymbol{\Xi}_{ct} = \boldsymbol{\mathcal{L}}_{ct}^{\mathrm{T}}\boldsymbol{\mathcal{L}}_{ct} = (5\times10^{3})\mathbf{1}_{6\times6} \quad , \quad \boldsymbol{\Xi}_{ds} = \boldsymbol{\mathcal{L}}_{ds}^{\mathrm{T}}\boldsymbol{\mathcal{L}}_{ds} = (5\times10^{2})\mathbf{1}_{6\times6}$$

$$\mathcal{P}_{\mathrm{f}} = \begin{bmatrix} \mathcal{P}_{\mathrm{f},1} & \mathcal{P}_{\mathrm{f},2} \\ \mathcal{P}_{\mathrm{f},2} & \mathcal{P}_{\mathrm{f},3} \end{bmatrix}$$

where $\boldsymbol{\Xi}_{ct} = \boldsymbol{\Xi}_{ct}^{\mathrm{T}} \geq \mathbf{0}$ and $\boldsymbol{\Xi}_{ds} = \boldsymbol{\Xi}_{ds}^{\mathrm{T}} \geq \mathbf{0}$ serve to weight Eq. (64), $\boldsymbol{\mathcal{P}}_{\mathrm{f},1} = \mathbf{1}_{3\times 3}$, $\boldsymbol{\mathcal{P}}_{\mathrm{f},2} = (10^{1})\mathbf{1}_{3\times 3}$, and $\boldsymbol{\mathcal{P}}_{\mathrm{f},3} = (10^{2})\mathbf{1}_{3\times 3}$. Lastly, the continuous-time and discrete-time positive control gains used in Eqs. (66) and (68), the utilization of which ensure input strict passivity via Eqs. (29) and (32), are tuned to $\gamma_{ct} = 8\times 10^{-1}$ and $\gamma_{ds} = 5\times 10^{-7}$ respectively.

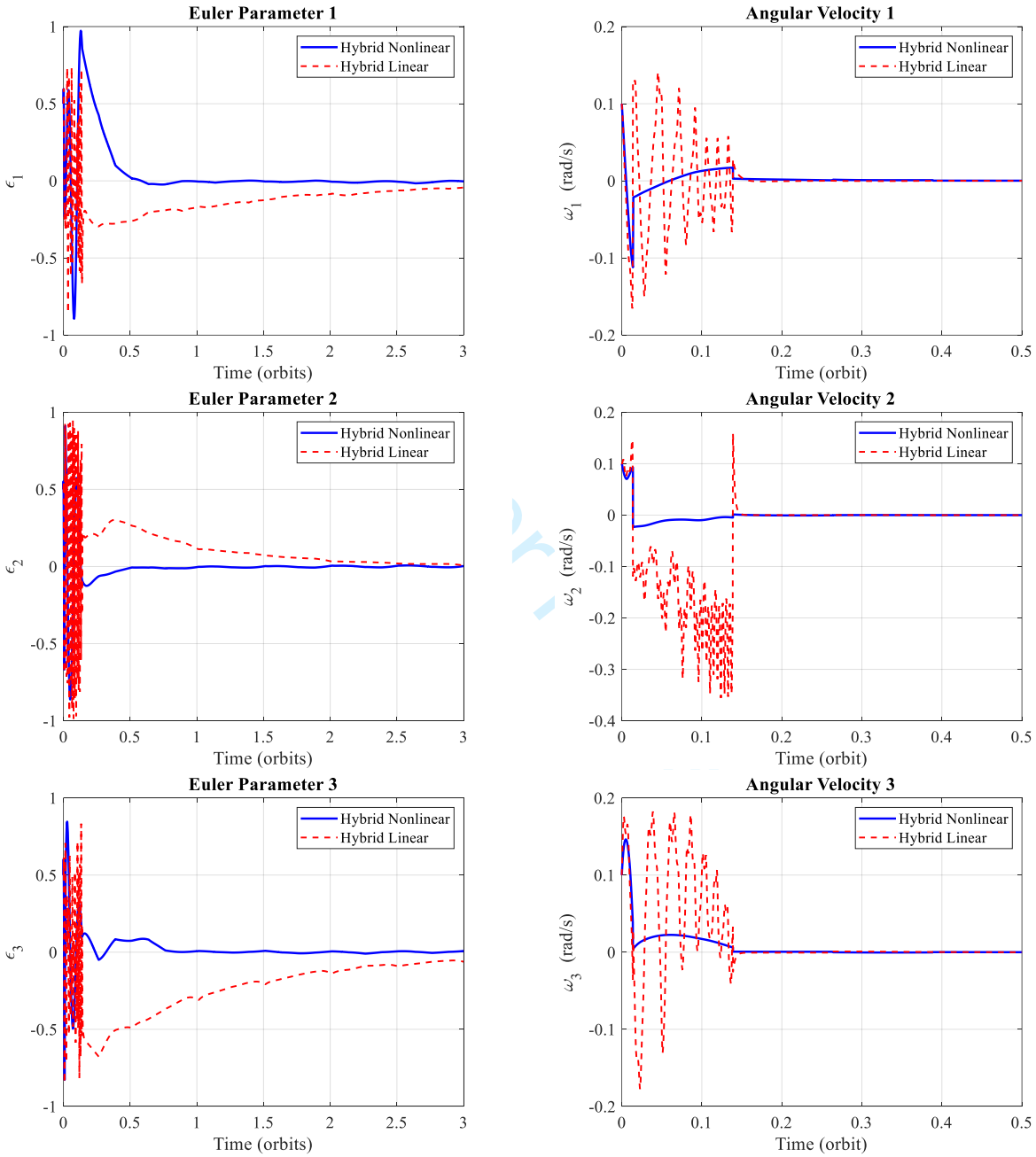

Fig. 4. Time histories of Euler parameters (left column) and angular velocity components (right column) for hybrid nonlinear and linear passivity-based attitude control schemes with dynamic compensator

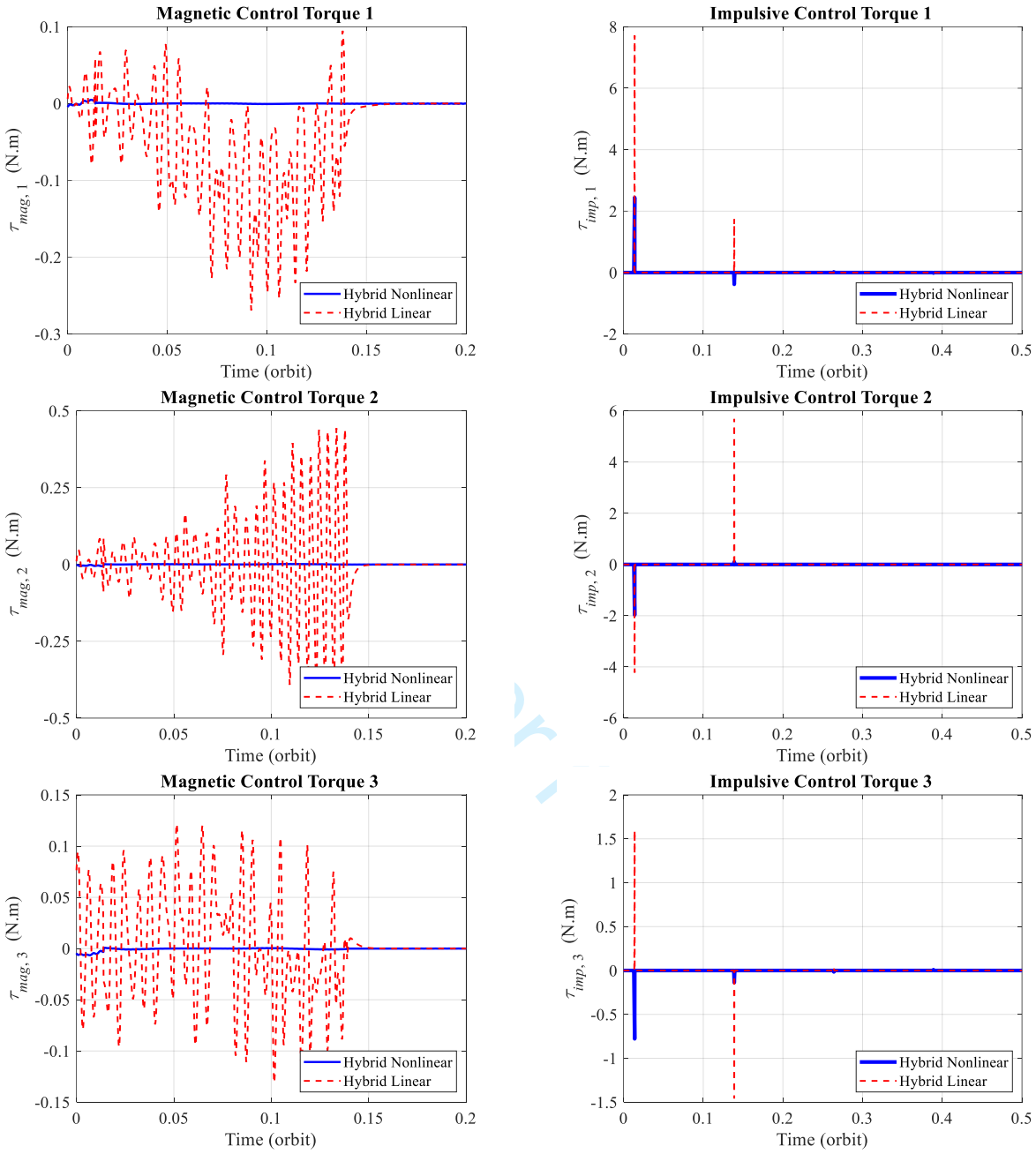

Fig. 5. Time histories of magnetic (left column) and impulsive (right column) control torques for hybrid nonlinear and linear passivity-based attitude control schemes with dynamic compensator

The simulation results, which present how the closed-loop attitude control system endowed with the hybrid nonlinear passivity-based dynamic compensator in its feedback loop responds to the initial conditions $\boldsymbol{\varepsilon}_0 = [0.5 \quad 0.5 \quad 0.5]^{\mathrm{T}}$, $\eta_0 = 0.5$, and $\boldsymbol{\omega}_0 = [0.1 \quad 0.1 \quad 0.1]^{\mathrm{T}}$ rad/s, are shown in Figs. 4 and 5 along with Table 2. As is expected, by increasing γ_{ct}, γ_{ds}, $\boldsymbol{Q}_{ct}$, and $\boldsymbol{Q}_{ds}$ (while $\boldsymbol{R}_{ct}$ and $\boldsymbol{R}_{ds}$ are decreased or remain constant), the resultant controller drives $\boldsymbol{\varepsilon}$ and $\boldsymbol{\omega}$ to zero faster in the presence of external disturbance torques. This improved performance

occurs, however, at the expense of larger magnetic dipole moments and impulsive thrusts, which are practically undesirable.

Figures 4 and 5 depict the performance of the hybrid nonlinear attitude control system with a dynamic compensator in terms of system response and control action as against the hybrid linear control, highlighting the superiority of the proposed nonlinear control design approach in the transient behavior, the settling time of which for $\boldsymbol{\varepsilon}$ is less than one orbit as opposed to five orbits for the linear scheme, and the control effort collaboratively made by magnetic torquers and thrusters to stabilize the system in the presence of external disturbance torques. Specifically, Fig. 5 shows considerable reduction in both magnetic and impulsive control torques applied by the magnetic torquers and thrusters respectively when the attitude control system is equipped with a nonlinear controller.

Table 2. Functional performance of hybrid nonlinear attitude control scheme equipped with dynamic compensator in comparison to hybrid linear and magnetic-only nonlinear control laws

	Parameter	$\mathcal{E}$	$\overline{\lVert\phi\rVert}$	$\overline{\lVert\omega\rVert}$	$\overline{\lVert\tau_{mag}\rVert}$	$\overline{\lVert\tau_{imp}\rVert}$
Control Policy	Hybrid Nonlinear Passive (**HNP**)	2.08×10^{12}	3.07×10^{-1}	5.35×10^{-3}	2.30×10^{-4}	2.94×10^{-1}
	Hybrid Linear Passive (**HLP**)	1.22×10^{16}	3.84×10^{-1}	2.11×10^{-2}	1.87×10^{-2}	9.88×10^{-1}
	Magnetic Nonlinear Passive (**MNP**)	7.45×10^{12}	5.89×10^{-1}	1.12×10^{-2}	5.14×10^{-4}	-
Improvement	**HNP** as compared to **HLP**	99.98 %	20.09 %	74.62 %	98.77 %	70.30 %
	HNP as compared to **MNP**	72.06 %	47.98 %	52.12 %	55.21 %	-
	MNP as compared to **HLP**	99.94 %	53.63 %	46.99 %	97.25 %	-

Table 2 also summarizes and compares the quantities resulted from quantitatively evaluating the performance of all three passivity-based attitude controllers via the RMS norms given by Eqs. (81) and (82). As is apparent, the numerical results demonstrate the superiority of the proposed hybrid nonlinear controller as against the other two control architectures. For instance, $\mathcal{E}$ and $\boldsymbol{\tau}_{mag}$, the contributions of which are significant in the feasibility of a control framework proposed for attitude regulation purposes, are enhanced by at least 97 percent. Whereas the magnetic dipole moments required by the proposed hybrid nonlinear controller for regulating the spacecraft attitude motion is only $2.30\times10^{-4}\ \mathrm{N\cdot m}$, which corresponds to $\boldsymbol{m} = 9.03\,\mathrm{A\cdot m^2}$ over 15 orbits and therefore offers reasonable values for near-Earth missions as mentioned in Refs. [14, 15], the hybrid linear control architecture needs torque rods capable of $691.06\,\mathrm{A\cdot m^2}$ at the expense of an inevitable increase in the dimensions and weight of the attitude control system

(via increasing $\mathcal{N}$ and $\mathcal{A}$), which is obviously impossible in practice. Moreover, impulsive control torques produced by thrusters are noticeably reduced from 9.88×10^{-1} to 2.94×10^{-1} N·m, a dramatic enhancement of 70.30 percent, when the linear control policy is replaced by the proposed nonlinear approach. As a consequence, the required onboard expendable fuels are significantly decreased, thereby extending mission life.

C. Measurement Noise Effects

This section aims to evaluate the immunity of the resultant closed-loop attitude dynamics, which separately utilize the hybrid nonlinear passivity-based controllers developed in Secs. III.D and III.E, to erroneous state knowledge originating from the attitude and rate measurements contaminated by noise effects. With this objective in view, this paper employs the approach proposed in Ref. [37] Sec. 25.1.5 to simulate noise effects through perturbing the actual state vector $\boldsymbol{x}(t)$ by a randomly generated zero-mean Gaussian white noise vector in the form of $\boldsymbol{E}\sqrt{\boldsymbol{\Lambda}}\boldsymbol{\rho}$ as follows: $\tilde{\boldsymbol{x}}(t)=\boldsymbol{x}(t)+\boldsymbol{E}\sqrt{\boldsymbol{\Lambda}}\boldsymbol{\rho}$; where $\tilde{\boldsymbol{x}}(t)$ is the perturbed state vector and $\boldsymbol{\rho}\sim\mathcal{N}(\boldsymbol{0},\boldsymbol{1})\in\mathbb{R}^{7\times1}$ denotes a vector of random numbers (i.e. a standard normal distribution) regenerated at each time step. By constructing the covariance matrix of the noise distribution in the form of $\boldsymbol{\Sigma}=\boldsymbol{E}\boldsymbol{\Lambda}\boldsymbol{E}^{\mathrm{T}}$ and then setting it equal to the variance parameters associated with the attitude and rate measurements as $\boldsymbol{\Sigma}=diag\left\{\sigma_{\boldsymbol{\varepsilon}}^2\boldsymbol{1}_{3\times3}\quad\sigma_{\eta}^2\quad\sigma_{\boldsymbol{\omega}}^2\boldsymbol{1}_{3\times3}\right\}$, $\boldsymbol{\Lambda}$ and $\boldsymbol{E}$ are accordingly obtained by performing an eigenvalue decomposition on $\boldsymbol{\Sigma}$ (which is assumed to be constant). As a consequence, $\boldsymbol{\Lambda}=diag\left\{\lambda_i\right\}$ and $\boldsymbol{E}=row\left\{\boldsymbol{e}_i\right\}$ wherein λ_i and $\boldsymbol{e}_i$ with $i=1,...,7$ represent the eigenvalues and corresponding eigenvectors of $\boldsymbol{\Sigma}$ respectively. Continuous-time and discrete-time output dynamics of the following forms are therefore formulated to be directly fed to the controllers (See Fig. 1) in order to incorporate the attitude and rate measurements contaminated by noise effects into the closed-loop attitude dynamics:

$$\begin{cases}\boldsymbol{y}_{ct}(t)=\boldsymbol{h}_{ct}(\tilde{\boldsymbol{x}},t) & t\neq t_k\\ \boldsymbol{y}_{ds,k}\ =\boldsymbol{h}_{ds}(\tilde{\boldsymbol{x}}_k^-,t)+\boldsymbol{j}_{ds}(\tilde{\boldsymbol{x}}_k^-,t)\boldsymbol{u}_{ds,k} & t=t_k\end{cases}\tag{83}$$

Assuming an attitude determination algorithm founded upon a combination of sensor inputs including a fluxgate magnetometer and the Global Positioning System (GPS), the variance parameters associated with the attitude and rate measurements are, respectively, set to 10^{-10} and 10^{-8} in this paper. This set of quantities, the selection of which is based upon the characteristics of the indicated attitude sensors, suggests mean values of approximate order 3×10^{-5}

and 3×10^{-4} rad/s for the quaternions and angular velocity components respectively through which measurements are contaminated by noise of largely exaggerated values for most spacecraft.

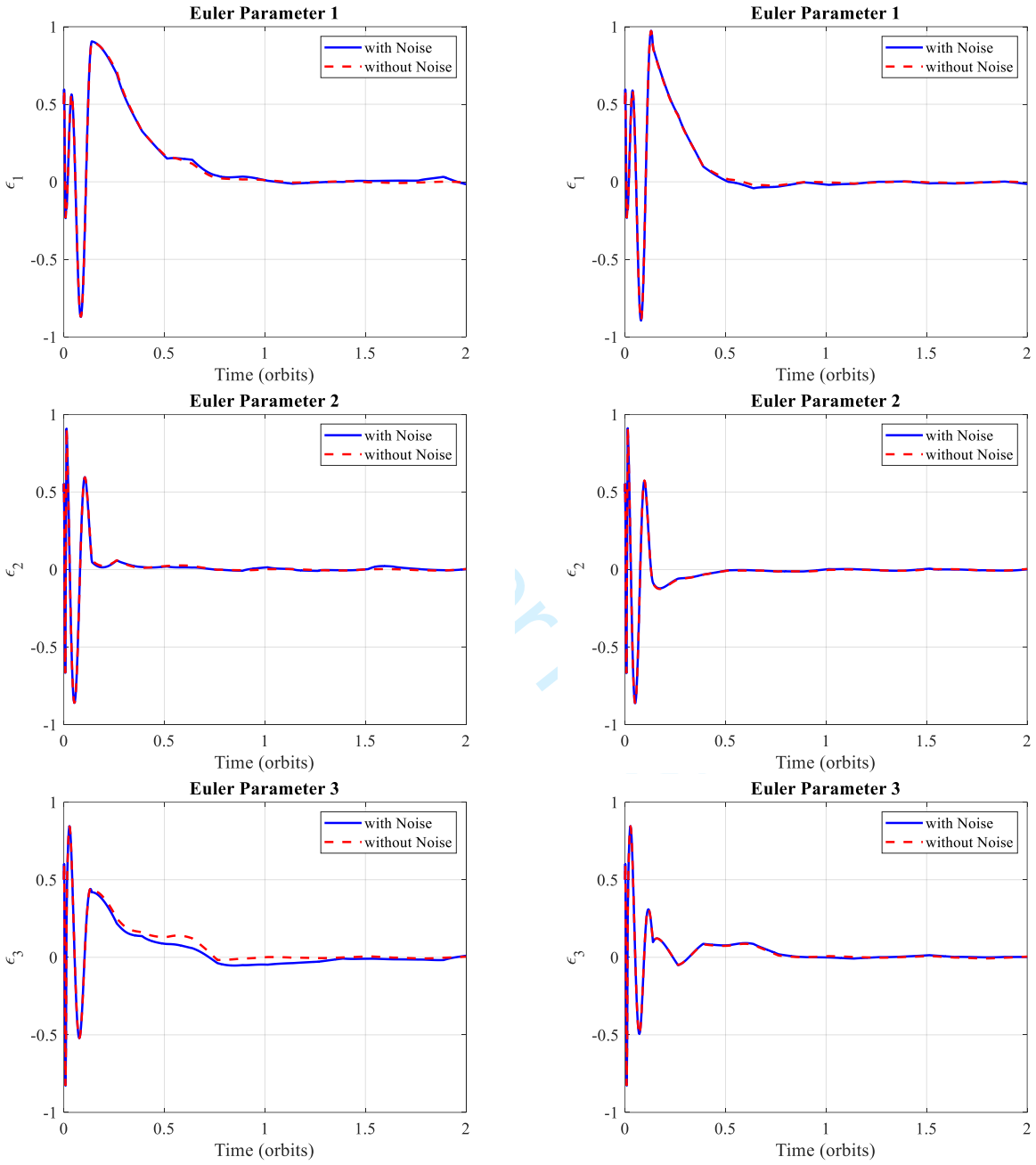

Fig. 6. Time histories of Euler parameters with and without measurement noise for hybrid nonlinear passivity-based attitude control scheme with static (left column) and dynamic (right column) compensators

Figure 6 demonstrates how the proposed hybrid nonlinear passivity-based static and dynamic compensators respond to measurement noise effects in the closed-loop attitude dynamics under the influence of the initial conditions $\boldsymbol{\varepsilon}_0 = \begin{bmatrix}0.5 & 0.5 & 0.5\end{bmatrix}^{\mathrm{T}}$, $\eta_0 = 0.5$, and $\boldsymbol{\omega}_0 = \begin{bmatrix}0.1 & 0.1 & 0.1\end{bmatrix}^{\mathrm{T}}$ rad/s. As is evident, both control architectures

exhibit reasonable immunity to sensor noise in view of the unrealistic values of perturbation selected to simulate a worst-case scenario. However, the attitude control system which employs the dynamic compensator developed in Sec. III.E demonstrates superior performance in comparison to the static compensator due to its dynamic time-varying nature when the state measurements are perturbed by sensor noise. The dynamic compensator is therefore recommended to use in the closed-loop dynamics when a significant source of measurement noise is expected.

VII. Conclusion

Two novel passivity-based control design frameworks for hybrid nonlinear time-varying dynamical systems involving an interacting mixture of continuous-time and discrete-time dynamics have been developed in this paper. By characterizing dissipativeness in terms of system dynamics and a generalized energy function via the hybrid Kalman-Yakubovich-Popov (KYP) conditions, a three-step control design procedure was proposed in compliance with the passivity theorem to render closed-loop dynamics stable. The proposed hybrid control architectures were subsequently exploited to regulate the attitude motion of spacecraft influenced by magnetic and impulsive sources of actuation. Simulation results demonstrated significant improvement in the performance of the proposed attitude control system in terms of transient response, steady-state behavior, and the required magnetic and impulsive control usage as compared to a hybrid linear approach in addition to the robust immunity of the resultant closed-loop dynamics to erroneous state knowledge originating from the measurements contaminated by noise effects. The proposed hybrid nonlinear passivity-based attitude control schemes possess several advantages: 1) the approximate control laws are in an explicit form of output feedback; 2) the control laws remain stable when the approximation is truncated at a finite degree of complexity; 3) the resultant control laws, the synthesis of which are based upon the full nonlinear kinematics and dynamics of the system, can be exploited over the entire operating range of the system; 4) instantaneous underactuation and gain limitations, as the main drawbacks inherently associated with the magnetically actuated attitude controllers, were resolved; and 5) the magnetic attitude control system collaboratively augmented by impulsive actuation is no longer restricted to high-inclined orbits and can therefore be applied to any orbit of arbitrary inclination, while simultaneously improving the speed of response and the accuracy of pointing.

References

[1] Haddad, W. M., Chellaboina, V., and Nersesov, S. G., *Impulsive and Hybrid Dynamical Systems*, Princeton University Press, Princeton, NJ, 2006, Chaps. 1, 3 and 6.

[2] Desoer, C. A., and Vidyasagar, M., *Feedback Systems: Input-Output Properties*, Academic Press, New York, 1975, Chap. 6, pp. 168–227.

[3] Popov, V. M., "Absolute Stability of Nonlinear Systems of Automatic Control," *Automation and Remote Control*, Vol. 22, No. 8, Aug. 1961, pp. 961–979.

[4] Yakubovich, V. A., "The Solution of Certain Matrix Inequalities in Automatic Control Theory," *Soviet Mathematics*, Vol. 3, No. 2, 1962, pp. 620–623.

[5] Kalman, R. E., "Lyapunov Functions for the Problem of Lur'e in Automatic Control," *Proceedings of the National Academy of Sciences of the USA*, Vol. 49, No. 2, Feb. 1963, pp. 201–205.

[6] Willems, J. C., "Dissipative Dynamical Systems, Part I: General Theory," *Archive for Rational Mechanics and Analysis*, Vol. 45, No. 5, Jan. 1972, pp. 321–351. doi: 10.1007/BF00276493

[7] Willems, J. C., "Dissipative Dynamical Systems, Part II: Linear Systems with Quadratic Supply Rates," *Archive for Rational Mechanics and Analysis*, Vol. 45, No. 5, Jan. 1972, pp. 352–393. doi: 10.1007/BF00276494

[8] Moylan, P. J., "Implications of Passivity in a Class of Nonlinear Systems," *IEEE Transactions on Automatic Control*, Vol. 19, No. 4, 1974, pp. 373–381. doi: 10.1109/tac.1974.1100603

[9] Hill, D. J., and Moylan, P. J., "The Stability of Nonlinear Dissipative Systems," *IEEE Transactions on Automatic Control*, Vol. 21, No. 5, Oct. 1976, pp. 708–711. doi: 10.1109/TAC.1976.1101352

[10] Hill, D. J., and Moylan, P. J., "Stability results for nonlinear feedback systems," *Automatica*, Vol. 13, No. 4, 1977, pp. 377–382. doi: 10.1016/0005-1098(77)90020-6

[11] Haddad, W. M., Chellaboina, V., and Kablar, N. A., "Non-Linear Impulsive Dynamical Systems. Part I: Stability and Dissipativity," *International Journal of Control*, Vol. 74, No. 17, 2001, pp. 1631–1658. doi: 10.1080/00207170110081705

[12] Vatankhahghadim, B., and Damaren, C. J., "Magnetic Attitude Control with Impulsive Thrusting using the Hybrid Passivity Theorem," *Journal of Guidance, Control, and Dynamics*, Vol. 40, No. 8, Aug. 2017, pp. 1860–1876. doi:10.2514/1.G002375

[13] Wertz, J. R., *Spacecraft Attitude Determination and Control*, D. Reidel Publishing, The Netherlands, 1978, Chaps. 5 and 19.

[14] Sidi, M. J., *Spacecraft Dynamics and Control: A Practical Engineering Approach*, Cambridge University Press, Cambridge, England, U.K., 1997, Chap. 7.

[15] Markley, F. L., and Crassidis, J. L., *Fundamentals of Spacecraft Attitude Determination and Control*, Springer, New York, 2014, Chap. 7.

[16] Avanzini, G., and Giulietti, F., "Magnetic Detumbling of a Rigid Spacecraft," *Journal of Guidance, Control, and Dynamics*, Vol. 35, No. 4, July–Aug. 2012, pp. 1326–1334. doi: 10.2514/1.53074

[17] Camillo, P. J., and Markley, F. L., "Orbit-Averaged Behavior of Magnetic Control Laws for Momentum Unloading," *Journal of Guidance, Control, and Dynamics*, Vol. 3, No. 6, 1980, pp. 563–568. doi: 10.2514/3.19725

[18] Silani, E., and Lovera, M., "Magnetic Spacecraft Attitude Control: A Survey and Some New Results," *Control Engineering Practice*, Vol. 13, No. 3, March 2005, pp. 357–371. doi: 10.1016/j.conengprac.2003.12.017

[19] Lovera, M., and Astolfi, A., "Spacecraft Attitude Control Using Magnetic Actuators," *Automatica*, Vol. 40, No. 8, 2004, pp. 1405–1414. doi: 10.1016/j.automatica.2004.02.022

[20] de Ruiter, A. H. J., "A Fault-tolerant Magnetic Spin Stabilizing Controller for the JC2Sat-FF Mission," *Acta Astronautica*, Vol. 68, No. 1–2, Jan.–Feb. 2011, pp. 160–171. doi: 10.1016/j.actaastro.2010.07.012

[21] Lovera, M., de Marchi, E., and Bittanti, S., "Periodic Attitude Control Techniques for Small Satellites with Magnetic Actuators," *IEEE Transactions on Control Systems Technology*, Vol. 10, No. 1, Jan. 2002, pp. 90–95. doi:10.1109/87.974341

[22] Arduini, C., and Baiocco, P., "Active Magnetic Damping Attitude Control for Gravity-Gradient Stabilized Spacecraft," *Journal of Guidance, Control, and Dynamics*, Vol. 20, No. 1, Jan.–Feb. 1997, pp. 117–122. doi: 10.2514/2.4003

[23] Forbes, J. R. and Damaren, C. J., "Linear Time-varying Passivity-based Attitude Control Employing Magnetic and Mechanical Actuation," Journal of Guidance, Control, and Dynamics, Vol. 34, No. 5, Sep.–Oct. 2011, pp. 1363–1372. doi: 10.2514/1.51899

[24] Lovera, M., "Optimal Magnetic Momentum Control for Inertially Pointing Spacecraft," *European Journal of Control*, Vol. 7, No. 1, 2001, pp. 30–39. doi: 10.1016/S0947-3580(01)70936-3

[25] Pulecchi, T., and Lovera, M., "Attitude Control of Spacecraft with Partially Magnetic Actuation," *IFAC Proceedings Volumes*, Vol. 40, No. 7, 2007, pp. 609–614. doi: 10.3182/20070625-5-FR-2916.00104

[26] Vatankhahghadim, B., and Damaren, C. J., "Optimal Combination of Magnetic Attitude Control with Impulsive Thrusting," *Journal of Guidance, Control, and Dynamics*, Vol. 39, No. 10, Oct. 2016, pp. 2391–2398. doi: 10.2514/1.G001664

[27] Kim, Y., and Deraspe, G., "Resolving RADARSAT-1 Momentum Wheels Failure Problem," *54th International Astronautical Congress of the International Astronautical Federation*, IAC-03-U.4.04, Bremen, Germany, Sept.Oct. 2003.

[28] Sharifi, E., and Damaren, C. J., "Passivity-based Control Design Frameworks for Hybrid Nonlinear Time-varying Dynamical Systems," *International Journal of Robust and Nonlinear Control*, 2023, 1-21. doi: 10.1002/rnc.6818

[29] Fletcher, C. A. J., *Computational Galerkin Methods*, Springer Series in Computational Physics, Springer, New York, 1984.

[30] Quarteroni, A., Sacco, R., and Saleri, F., *Numerical Mathematics*, Springer–Verlag, New York, 2000.

[31] Benhabib, R. J., Iwens, R. P., and Jackson, R. L., "Stability of Large Space Structure Control Systems Using Positivity Concepts," *Journal of Guidance, Control, and Dynamics*, Vol. 4, No. 5, Sept.–Oct. 1981, pp. 487–494. doi: 10.2514/3.56100

[32] Sobiesiak, L. A., and Damaren, C. J., "Optimal Continuous/Impulsive Control for Lorentz-Augmented Spacecraft Formations," *Journal of Guidance, Control, and Dynamics*, Vol. 38, No. 1, 2015, pp.151–156. doi: 10.2514/1.G000334

[33] Hughes, P. C., *Spacecraft Attitude Dynamics*, Wiley, New York, 1986.

[34] Beard, R., Saridis, G., and Wen, J., "Galerkin Approximations of the Generalized Hamilton-Jacobi-Bellman Equation," *Automatica*, Vo. 33, No. 12, 1997, pp. 2159–2177. doi: 10.1016/S0005-1098(97)00128-3

[35] Beard, R., Saridis, G., and Wen, J., "Improving the Performance of Stabilizing Controls for Nonlinear Systems," *IEEE Control Systems Magazine*, Vol. 16, No. 5, Oct. 1996, pp. 27–35. doi: 10.1109/37.537206

[36] Beard, R., and McLain, T., "Successive Galerkin Approximation Algorithms for Nonlinear Optimal and Robust Control," *International Journal of Control*, Vol. 71, No. 5, 1998, pp. 717–743. doi: 10.1080/002071798221542

[37] de Ruiter, A. H. J., Damaren, C. J., and Forbes, J. R., *Spacecraft Dynamics and Control: An Introduction*, Wiley, NJ, 2013.